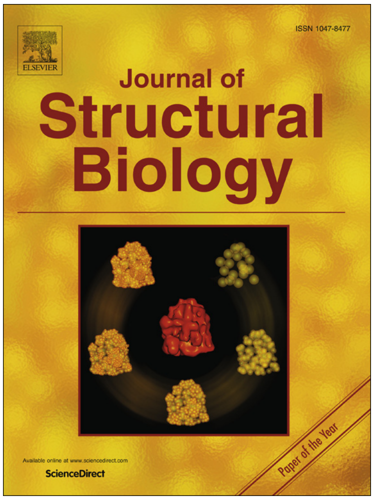

Analysis of distinct molecular assembly complexes of keratin K8 and K18 by hydrogen-deuterium exchange

Aiswarya Premchandar, Anna Kupniewska, Krzysztof Tarnowski, Norbert Mücke, Monika Mauermann, Magdalena Kaus–Drobek, Aleksander Edelman, Harald Herrmann, Michał Dadlez

PII: S1047-8477(15)30079-4
DOI: http://dx.doi.org/10.1016/j.jsb.2015.10.001
Reference: YJSBI 6791

To appear in: *Journal of Structural Biology*

Received Date: 16 July 2015
Revised Date: 24 September 2015
Accepted Date: 1 October 2015

Please cite this article as: Premchandar, A., Kupniewska, A., Tarnowski, K., Mücke, N., Mauermann, M., Kaus–Drobek, M., Edelman, A., Herrmann, H., Dadlez, M., Analysis of distinct molecular assembly complexes of keratin K8 and K18 by hydrogen-deuterium exchange, *Journal of Structural Biology* (2015), doi: http://dx.doi.org/10.1016/j.jsb.2015.10.001

This is a PDF file of an unedited manuscript that has been accepted for publication. As a service to our customers we are providing this early version of the manuscript. The manuscript will undergo copyediting, typesetting, and review of the resulting proof before it is published in its final form. Please note that during the production process errors may be discovered which could affect the content, and all legal disclaimers that apply to the journal pertain.

Analysis of distinct molecular assembly complexes of keratin K8 and K18 by hydrogen-deuterium exchange

Aiswarya Premchandar[1], Anna Kupniewska[1], Krzysztof Tarnowski[1],
Norbert Mücke[3], Monika Mauermann[4], Magdalena Kaus–Drobek [1], Aleksander Edelman[5],
Harald Herrmann[4], Michał Dadlez [1, 2]

[1] *Institute of Biochemistry and Biophysics, Polish Academy of Sciences, Pawińskiego 5A, 02–106 Warsaw, Poland*
[2] *Warsaw University, Biology Department, Institute of Genetics and Biotechnology, Miecznikowa 3, Warsaw, Poland*
[3] *Biophysics of Macromolecules, and* [4] *Molecular Genetics, German Cancer Research Center (DKFZ), Im Neuenheimer Feld 280, D–69120 Heidelberg, Germany*
[5]*INSERM U1151, Université Paris Descartes, Paris, France*

Running title: *Hydrogen–deuterium exchange in keratin oligomers and filaments*

*Corresponding author. Michał Dadlez.
Institute of Biochemistry and Biophysics, Department of Biophysics, 02–106 Warsaw Tel.: (+48) 22 5923 471; fax: (+48) 22 658 4766; E–mail: michald@ibb.waw.pl

Abstract

Keratins are intermediate filament (IF) proteins that form complex filament systems in epithelial cells, thus serving as scaffolding elements and mechanical stress absorbers. The building blocks of keratin IFs are parallel coiled–coil dimers of two distinct sequence–related proteins distinguished as type I and type II keratins. To gain more insight into their structural dynamics, we resorted to hydrogen–deuterium exchange mass spectrometry of keratins K8 and K18, which are characteristic for simple epithelial cells. Using this powerful technique not employed with IFs before, we mapped patterns of protected versus unprotected regions in keratin complexes at various assembly levels. In particular, we localized protein segments exhibiting different hydrogen exchange patterns in tetramers versus filaments. We observed a general pattern of precisely positioned regions of stability intertwining with flexible regions, mostly represented by the non–α–helical segments. Notably, some regions within the coiled–coil domains are significantly more dynamic than others, while the IF–consensus motifs at the end domains of the central α–helical "rod" segment, which mediate the "head–to–tail" dimer–dimer interaction in the filament elongation process, become distinctly more protected upon formation of filaments. Moreover, to gain more insight into the dynamics of the individual keratins, we investigated the properties of homomeric preparations of K8 and K18. The physiological importance of keratins without a partner is encountered in both pathological and experimental situations when one of the two species is present in robust excess or completely absent, such as in gene–targeted mice.

Keywords: Intermediate filament, Cytoskeleton, Keratin, Electron microscopy (EM), Hydrogen–deuterium exchange

Abbreviations: AUC, analytical ultracentrifugation; EM, electron microscopy; HDX, hydrogen–deuterium exchange; HMO, homomeric; HRO, heteromeric; IF, intermediate filaments; K8, keratin 8; K18, keratin 18; LC, liquid chromatography; MS, mass spectrometry; ULF, unit–length filament; EPR, electron paramagnetic resonance

1. Introduction

The principal components of the intermediate filament (IF) cytoskeleton in simple epithelial cells are keratin K8 and keratin K18 (Moll et al., 2008). The central function of this keratin filament system is to provide protection against mechanical and physiological stress (Omary et al., 2009). Keratins differ from the other members of the cytoplasmic IF protein family such as vimentin and desmin by forming obligate hetero–coiled coils with one monomer from sequence homology class I (SHC I or type I), i.e. K9–K28 and K31–K40, and one monomer from SHC II (or type II), i.e. K1–K8 and K71–K86 (Herrmann and Aebi, 2000; Moll et al., 2008; Strelkov et al., 2003). Like all IF proteins, keratins exhibit a tripartite organization with a central α–helical, coiled–coil forming "rod" domain that is flanked by non–α–helical, intrinsically disordered amino–terminal "head" and carboxy–terminal "tail" domains (Figure 1A). Between different IF proteins, the α–helical domains match by the amino acid number, whereas the head and tail domains extensively vary in length and amino acid composition. In contrast, the structural organization of the α–helical rod is highly conserved, exhibiting major segments of 7–residue (heptad) and 11–residue (hendecad) repeats that are interrupted at identical sites by non–α–helical linkers (Chernyatina et al., 2015; Herrmann and Aebi, 2004; Herrmann et al., 2009).

IFs are notoriously insoluble under physiological conditions and for their biochemical characterization, they have to be denatured using agents such as urea. The basic building block of IFs is a dimer of two molecules arranged as a parallel coiled–coil (Figure 1B). A stable dimer forms spontaneously without any need for chaperones when the completely unfolded proteins are dialyzed from 8 M to 6 M urea. Analytical ultracentrifugation has verified this intrinsic property of vimentin IFs (Herrmann et al., 1996; Lichtenstern et al., 2012). By further lowering the urea concentration to 5 M urea, two dimers assemble into an anti–parallel, half–staggered tetrameric complex (Herrmann et al., 2002; Parry and Steinert, 1999; Parry, 2005; Szeverenyi et al., 2008). The relative orientation of the individual monomers in a tetramer has been resolved by chemical cross–linking (Parry D.A.D., 1995) and in some more detail by X–ray crystallization in combination with EPR–techniques (Aziz et al., 2012; Chernyatina et al., 2012). Under low ionic strength conditions, the tetramer is stable. Although keratins are obligate heterodimers in filaments, on their own they interact to different degrees, although they do not assemble into IFs. K8 was demonstrated to form homodimers and with increased protein concentration, higher order complexes; in contrast, K18 forms monomers and only at higher protein concentration assembles further (Lichtenstern et al., 2012). These properties may be indeed of interest in cellular situations of unbalanced protein expression, such as encountered in liver diseases (Guldiken et al., 2015).

The formation of K8/K18 complexes and their assembly into filaments has been extensively studied by analytical ultracentrifugation, viscometry, and electron microscopy (Hatzfeld and Franke, 1985; Lichtenstern et al., 2012). To investigate the assembly properties of keratins with respect to the subunit dynamics, we used hydrogen–deuterium exchange (HDX) monitored by mass spectrometry (MS) to obtain insights into the dynamic structural properties of full–length keratins in solution. We studied and compared defined oligomeric states of keratins by selecting appropriate pH and ionic strength buffers. HDX coupled to MS (HDX–MS) is an established alternative method of protein structure analysis (Marcsisin and Engen, 2010; Wales and Engen, 2006). This technique allowed us to overcome the limitations of the classic methods, like the molecular mass limit and high protein concentration required for NMR or the necessity to obtain a protein crystal. HDX–MS probes the susceptibility of main–chain amide protons to exchange with bulk solvent. Thus, it allows mapping the hydrogen–bonded network stability in different regions of the protein and thereby differentiates their well–structured and flexible regions. This methodology allows studying a protein or its higher order complexes in native buffer conditions at micromolar concentrations, in principle without mass limit. The method, however, is categorized as a medium–level resolution technique since the exchange is measured for proteolytic peptides of the protein of interest and not for single amide protons.

HDX–MS was recently used to study coiled–coil structure dynamics, for example, the triple coiled–coil of fibrinogen (Marsh et al., 2013) and the troponin complex double coiled–coil (Bou–Assaf et al., 2011). Fibrinogen displayed substantial differences in dynamics along its sequence, with the terminal regions more stable than the medium segments of the coiled–coil, which in some cases showed no measurable protection against the exchange. NMR can also monitor HDX at residue level resolution, but up to now it has only been applied to study coiled–coil dynamics of short peptides (Goodman and Kim, 1991).

In this study, we have applied HDX–MS to keratins K8 and K18 and thereby obtained detailed insight into the in–solution structural properties of these proteins at various organizational levels. We have mapped the stable and flexible regions in K8 and K18 preparations and thus identified segments that reveal differences in HDX upon heterocomplex formation and furthermore upon transition from tetramers to filaments. These data may furthermore serve as a generic model for the assemblies of other types of IF proteins and thereby provide new insights into their general dynamic structural properties.

2. Materials and Methods

2.1. Protein purification and oligomer/filament assembly

Keratins K8 and K18 were expressed in BL21 (DE3) bacteria using the pET system. We employed pET24a for K8 and pET23a for K18 using the NdeI site for the start methionine. The proteins were isolated from inclusion bodies as previously reported(Nagai and Thøgersen, 1987), with modifications as described (Herrmann et al., 1992). Protein pellets were dissolved in *column buffer* (10 mM Tris–HCl, pH 7.5, 1 mM DTT, 1 mM EDTA, 0.1 mM EGTA, freshly deionized 8 M urea) and cleared by centrifugation in a 50 Ti rotor at 35,000 rpm in a Beckman ultracentrifuge for 1 h at 20 °C. Proteins were purified by ion–exchange chromatography. Using Q Sepharose Fast Flow in 50 mL Econo–columns (Bio–Rad) with 15 mL of settled resin, bound proteins were eluted with a gradient of 0 M to 0.3 M NaCl in column buffer (100 mL). The eluted fractions were analyzed by SDS–PAGE, and appropriate fractions were pooled for further purification. Before they were applied to an SP Sepharose Fast Flow column, the combined fractions were diluted 1:1 with column buffer to reduce the salt concentration. Bound proteins were eluted as described for the Q–Sepharose Fast Flow column and desired fractions were identified by SDS–PAGE. Pooled keratin fractions were subjected to SDS–PAGE and immunoblot analysis to verify their purity. For stability control, keratin aliquots were dialyzed into 2 mM Tris–HCl, pH 9.0. Only those samples that showed no degradation bands on the SDS–PAGE were used for further analysis (Supplementary Figure S1). Renaturation of urea–denatured proteins was essentially performed as described previously (Herrmann et al., 2004a). Refolded proteins were concentrated using 10 kDa cut–off concentrators (Millipore) to obtain a final concentration of about 50 µM for individual keratins and 30 µM for the K8/K18 complex. The samples were centrifuged at 14,500 rpm in a bench–top centrifuge to remove any higher order aggregates. All experiments were carried out at room temperature. We initiated filament assembly in 2 mM Tris–HCl, pH 9.0 by the addition of one–tenth volume of 100 mM Tris–HCl, pH 7.5.

2.2. Analytical ultracentrifugation

Analytical ultracentrifugation (AUC) was performed in a Beckman analytical ultracentrifuge (model Optima XLA) equipped with an ultraviolet absorption optical system. Sedimentation velocity experiments were carried out in double–sector charcoal–Epon cells at 20 °C at 40,000 rpm. Scans were recorded at 230 nm using continuous scan mode and radial spacing of 0.003 cm. Absorbance scans were taken at 280 nm when the concentration of the sample was higher than 0.25 mg/mL. For the density and viscosity of the buffers, we assumed values as for water, so no correction to standard conditions (water, 20 °C) was needed. A partial specific volume of 0.712 mL/g for K8 and 0.713 mL/g for K18 was calculated using the program SEDNTERP V1.09, written by J. Philo, D. Hayes, T. Laue (http://www.jphilo.mailway.com/download.htm). Data were analyzed with DCDT+; V2.4.0, using the refined version of the derivative method (Philo, 2006) that implements the algorithms originally described in (Stafford, 1992).

2.3. Electron microscopy

In parallel to the HDX–MS experiments, for EM we prepared negatively stained specimens of keratins in the respective assembly condition described above. Specimen preparation was exactly as described with samples fixed in solution with 0.1% glutaraldehyde in the respective buffer and deposition times of the samples on the grid between 30 s and 2 min (Herrmann et al., 2004b). Grids were inspected using a Zeiss EM 900 (Carl Zeiss, Oberkochen, Germany).

2.4. Hydrogen–deuterium Exchange

In the first step of the analysis, the list of keratin peptides was established using a non–deuterated sample. 5 µL of the protein stock solution (30–50 µM) were diluted 10–fold by adding to 45 µL of one of the three H_2O reaction buffer: 1) 2 mM Tris–HCl, pH 9.0; 2) 5 mM Tris–HCl, pH 8.4; and 3) 10 mM Tris–HCl, pH 7.5.

This dilution yielded a final concentration of 3–5 µM, corresponding to 0.3–0.5 mg/mL of protein. The sample was then acidified by mixing with 10 µL of H_2O stop buffer (2 M glycine buffer, pH 2.5). The sample was digested online for 1.5 min using a 2.1 mm × 30 mm immobilized pepsin resin column (Porozyme, ABI, Foster City, CA) with 0.07% formic acid in water as the mobile phase (200 µL/min flow rate). The peptides were passed directly to the 2.1 mm × 5 mm C18 trapping column (ACQUITY BEH C18 VanGuard precolumn, 1.7 µm resin, Waters, Milford, MA). Trapped peptides were eluted onto a reversed phase column (Acquity UPLC BEH C18 column, 1.0 × 100 mm, 1.7 µm resin, Waters, Milford, MA) using a 8–40% gradient of acetonitrile in 0.1% formic acid at 40 µL/min, controlled by the nanoACQUITY Binary Solvent Manager. Total time of a single run was 13.5 min. All fluidics, valves, and columns were maintained at 0.5 °C using the HDX Manager (Waters, Milford, MA), with the exception of the pepsin digestion column, which was kept at 20 °C inside the temperature–controlled digestion column compartment of the HDX manager. The C18 column outlet was coupled directly to the ion source of SYNAPT G2 HDMS mass spectrometer (Waters, Milford, MA) working in Ion Mobility mode. Lock mass was activated and carried out using Leucine–enkephalin (Sigma). For protein identification, mass spectra were acquired in MS^E mode over the m/z range of 50–2000. The spectrometer parameters were as follows: ESI positive mode, capillary voltage 3 kV, sampling cone voltage 35 V, extraction cone voltage 3 V, source temperature 80 °C, desolvation temperature 175 °C, and desolvation gas flow 800 L/h. The spectrometer was calibrated using standard calibrating solutions.

Peptides were identified using ProteinLynx Global Server software (PLGS, Waters, Milford, MA). We used a randomized database, with PLGS parameters set at minimum fragment ions per peptide = 4 and a false–positive rate threshold of 4%. The list of identified peptides, containing peptide m/z, charge, retention time, and ion mobility/drift time was passed to the DynamX 2.0 hydrogen–deuterium data analysis program (Waters, Milford, MA).

HDX experiments were carried out as described for the non–deuterated sample, with the reaction buffer, prepared using D_2O (99.8% Cambridge Isotope Laboratories, Inc.), and pH (uncorrected meter reading) adjusted using DCl (Sigma). After mixing 5 µL protein stock with 45 µL D_2O reaction buffer, the exchange reactions were carried out for varied time periods, as specified in the text, at room temperature. The exchange was quenched by reducing the pH to 2.5 by adding the reaction mixture to stop buffer (2 M glycine buffer, pH 2.5) and cooling on ice. Immediately after quenching in the stop buffer, the sample was manually injected into the nanoACQUITY (Waters, Milford, MA) UPLC system. Subsequently, pepsin digestion and liquid chromatography (LC) and MS analysis were carried out exactly as described above for non–deuterated samples.

Two control experiments were performed to account for in– and out–exchange artifacts, as described previously (Kacprzyk-Stokowiec et al., 2014). In brief, to assess minimum exchange (in–exchange control), D_2O reaction buffer was added to stop buffer that had been cooled on ice prior to addition of protein stock, and this mixture was immediately subjected to pepsin digestion and LC–MS analysis as described above. The deuteration level in an in–exchange experiment was calculated as described below and denoted as 0% exchange (M_{ex}^0). For out–exchange analysis, 5 μL of protein stock was mixed with 45 μL of D_2O reaction buffer, incubated for 24 h, mixed with stop buffer and analyzed as described above. The deuteration level in an out–exchange experiment was calculated and denoted as 100% exchange (M_{ex}^{100}).

The above experimental scheme enabled us to obtain the same set of fragments from the control and HDX experiments. Each experiment was repeated three times, and the results represent the mean of these replicates.

2.5. HDX data analysis

The deuteration level for each peptide resulting from exchange was calculated in an automated way using DynamX 2.0 software, based on the peptide list obtained from the PLGS program, further on filtered in DynamX 2.0 program with the following acceptance criteria: minimum intensity threshold – 3000, minimum products per amino acids – 0.3. The analysis of the isotopic envelopes after exchange was carried out in DynamX 2.0 with the following parameters: RT deviation ± 15 s, m/z deviation ± 12.5 ppm, and drift time deviation ± 2 time bins. The average masses of peptides in the exchange experiment (M_{ex}) and the two control experiments (M_{ex}^0 and M_{ex}^{100}) obtained from the automated analysis were then verified by visual inspection. Ambiguous or overlapping isotopic envelopes were discarded from further analysis. Whenever a split isotopic envelope was observed, the separate M_{ex} values corresponding to each envelope were calculated using the MassLynx program.

Final data were exported to an Excel (Microsoft) spreadsheet for calculation of HDX mass shifts and fraction of exchange calculation. The percentage of relative deuterium uptake (% Deuteration) of a given peptide was calculated by taking into account both control values, following the formula:

$$\% \text{ Deuteration} = ((M_{ex} - M_{ex}^0) / (M_{ex}^{100} - M_{ex}^0))*100$$

Error bars for exchange fraction (f) were calculated as standard deviations of three independent experiments. The value of the difference in exchange (ΔHDX) between two conditions of interest was obtained by subtracting the fraction of exchange measured in these conditions. Errors for ΔHDX value were calculated as the square root of the sum of variances of the subtracted numbers. Fitting of the split isotopic envelopes to a sum of two distributions was carried out using the HXExpress (http://www.hxms.com/HXExpress/) program(Guttman et al., 2013). Final figures were plotted using OriginPro 8.0 (OriginLab) software.

3. Results

3.1. Oligomeric status of K8 and K18 as determined by AUC

We performed sedimentation velocity studies for K8/K18 hetero–oligomers (HRO) and the corresponding homomeric (HMO) preparations of K8 and K18 under ionic conditions that represent the stages of keratin assembly from soluble complexes to filaments: 1) in 2 mM Tris–HCl, pH 9.0, known to yield soluble complexes for K8, K18 and K8/K18 (Lichtenstern et al., 2012); 2) in 5 mM Tris–HCl, pH 8.4; and 3) in 10 mM Tris–HCl, pH 7.5, when keratins K8 and K18 assemble into long, regular filaments (Lichtenstern et al., 2012).We decided to explore the assembly state of K8 and K18 at 5mM Tris–HCl, pH 8.4 because it constitutes an intermediate state in their filament assembly. Thus, this state is encountered when the proteins are dialyzed from the tetrameric state (2mM Tris–HCl, pH 9.0) to filaments (10mM Tris–HCl, pH 7.5). The rationale to investigate this intermediate condition was to characterize a soluble association state closer to physiological conditions for future interaction studies with keratin–binding proteins, such as the chloride channel, CFTR, mutated in cystic fibrosis disease (Odolczyk et al., 2013).

Previous analyses, both by velocity sedimentation and equilibrium sedimentation studies, indicated that K8/K18 heteromeric complexes at pH 9.0 existed in the form of tetramers with *s*–values of 5.0 S at 0.15 mg/mL and 5.6 S at 0.7 mg/mL (Lichtenstern et al., 2012). Quite differently, K8 by itself formed dimers at low protein concentration, but its *s*–value shifted from 4.2 S to 6.1 S at 0.7 mg/mL, indicating some further interaction of dimers. Also, about 50% of K8 was present in complexes of 24 S at this higher protein concentration. K18 was monomeric with *s*–values of 2.8 and 2.6 S at 0.15 to 0.7 mg/mL, respectively, although the formation of higher sedimenting species was not followed (Lichtenstern et al., 2012).

For HDX experiments, we require stock protein concentrations of at least 3 mg/mL to perform a reliable peptide analysis after the ten–fold dilution of the samples with D_2O. Therefore, we analyzed the three sets of proteins (K8, K18, and K8/K18), in the concentration range, routinely used, i.e. 0.2 mg/mL. We also concentrated the proteins to between 3 and 6 mg/mL and then diluted them again ~20–fold to determine if the concentration regime affected the oligomeric state of the corresponding protein complexes. Moreover, we attempted to quantify the ratio of low to high molecular weight complexes under these particular conditions.

The authentic K8/K18 heterotetramer complexes sedimented in the range of 4.4 S to 6.5 S at pH 9.0, with about 30% of the protein sedimenting at higher *s*-values (Table 1). The concentration step did not have a marked effect on the sedimentation behavior (see values in Table 1 right to the backslash). At pH 8.4, sedimenting species with *s*-values of 4.7 to 4.8 and 6.6 to 6.7 S, respectively, were observed. Also under this pH regime, the prior concentration to 3 mg/mL followed by dilution did not significantly affect the sedimentation behavior of the soluble complexes. Again, up to 30% of the proteins were found in higher sedimenting fractions (Table 1). In contrast, at 10 mM Tris–HCl, pH 7.5, our standard filament formation condition for K8/K18 (Lichtenstern etal., 2012), massive filament formation occurred and AUC was therefore not applicable.

At pH 9.0, K8 sedimented at 3.7 and 3.9 S, respectively, representing 88% and 97% of the recorded protein; minor species were found at 12 to 17 S (Table 1). In contrast, in a run following a preconcentration-dilution step, the percentage of protein found in the low *s*–value range dropped significantly (Table 1). Hence, the concentrating regime caused an increase in higher–order complexes, stabilized probably by weak non-specific interactions, which did not dissociate completely upon dilution of the sample. For K18 at pH 9, a major fraction of the protein sedimented at 2.6 to 2.8 S, with higher sedimenting complexes appearing between 9 and 14 S (Table 1). Similar to K8, the concentration–dilution step did not significantly affect the *s*-values of the small sedimenting complexes but caused as well a significant reduction in the percentage of the low sedimenting complex (2.7 S) compared to the control without concentration–dilution step. Hence, the aggregates were maintained after dilution.

3.2. EM of soluble keratin complexes

To visualize the protein complexes of higher *s*–value, we analyzed negatively stained samples by transmission EM. Before application to the EM grid, samples were briefly fixed with 0.2 % glutaraldehyde in solution to prevent rearrangements of the protein complexes on the glow–discharged grid surface. From the inspection of large areas on several grids, we observed that K8 alone formed relatively regular rodlets, both at pH 8.4 (Figure 2A) and at pH 7.5 (not shown). Complexes in the size range of tetramers and higher oligomers were not visualized well under these conditions of imaging, although they were abundantly present, evident as a “background pattern” on the grid as seen before previously (Eichner et al., 1985; Franke et al., 1982) K18 formed similar–sized although slightly less regular structures (Figure 2B). Through the concentration steps, the outlines of these complexes were unaltered (Figure 2C, D).

3.3. Native K8/K18 filaments – a summary of structural features

For the assembly of various keratins, low ionic strength Tris–buffers of pH 7.2 to 7.5 are usually employed to generate single IFs (Coulombe and Fuchs, 1990; Hofmann et al., 2002; Lichtenstern et al., 2012). In contrast, at higher protein concentrations physiological ionic strength buffers induce immediate strong bundling of newly formed individual filaments (Lieleg et al., 2011). We have established here by EM that K8/K18 HROs form predominantly single filaments in 10 mM Tris–HCl buffer, pH 7.5, despite the fact that assembly was initiated at a relatively high protein concentration followed by ten–fold dilution with buffered D_2O (see also(Kayser et al., 2013)). We measured HDX of soluble keratin filaments after different times of incubation. The overall observed exchange was rapid, with the strongest differences seen between the patterns of exchange observed after a short incubation time (10 s). Figures 3A, E and 3B, F show the levels of deuteration of K8 and K18 in filaments, respectively. Data obtained for all identified peptides are shown illustrating an overall high coverage of protein sequence, the internal consistency of the results for peptides covering the same region, and a good reproducibility of the results obtained in triplicates. The color–coded representation in Figure 3E, F summarizes the exchange levels in different regions of the protein.

Already after 10 s of exchange, we observed full deuteration in most of the head domains and throughout the entire tail domains for both proteins in the filamentous state. This outcome indicates a lack of protection and thus, a lack of H–bonded structures in both the head and tail regions. Regions of the strongest protection are restricted to several peptides covering parts of the coiled–coil domain. For K8 (Figure 3A, E), these regions include the C–terminal segment of coil 1A, the whole coil 1B region and region 330–390 of coil 2B i.e. the coiled–coil forming segment. For K18 (Figure 3B, F), the slowest exchange was observed for C–terminal coil 1A, two regions of coil 1B, coil 2A and the 295–350 region of coil 2B. For other regions, we have observed intermediate levels of exchange. Of interest, intermediate levels of exchange were observed for both proteins in large regions of N–terminal coil 2B and in N–terminal coil 1A. For K8, the partly protected region included coil 2A while, for K18, it included the center of coil 1B and the C–terminus of coil 2B. All of these regions belong to the coiled–coil rod domain of keratin filaments, but our HDX study unequivocally shows substantial differences in the dynamics within the coiled–coil rod segment. The most prominent region lacking protection was the N–terminal half of coil 2B in both proteins. In contrast to a fully well–protected coil 1B in K8, the equally well–protected region in coil 2B was restricted to its central part, covering 60 aa in K8 and 55 aa in K18. In K8, the protection of linker L2 coalesced with the neighboring C–terminal coil 2A and the N–terminal coil 2B. For K18, the protection of L2 was similar to that of the neighboring N–terminal coil 2B. The HDX experiment, thus, uncovered substantial differences in the dynamics of different regions assigned to coiled–coil structures with the most prominent region of increased exchange encompassing the N–terminal part of coil 2B. In contrast, the head, tail, and L12 regions showed no signs of H–bonded structures in filaments. However, the short coil 1A was found to be partitioned into two regions: the less protected N–terminus and the fully protected C–terminus. These data compare well with the concept that coil 1A may be in open conformation as a reflection of its dynamic role during filament elongation (Meier et al., 2009; Parry et al., 2007).

3.4. Comparison of filaments and tetramers

By AUC, it had been noted that reconstitution of K8/K18 complexes into a 5 mM Tris–HCl buffer, pH 8.4, or 2 mM Tris–HCl buffer, pH 9.0, led to the formation of a mixture of tetramers and a smaller fraction of higher order oligomers. The prevalence of tetramers remained unchanged at pH 8.4 in samples subjected to a 10–fold concentration step. However at pH 9.0, the fraction of higher order oligomers in the 10–fold concentrated samples was slightly higher than in samples reconstituted directly into the protein concentration employed for the velocity runs (see above, and Table 1). This control was performed to reveal if the prior concentration of the samples for the 10–fold dilution with D_2O would lead to any notable aggregation of the keratins.

ACCEPTED

The overall pattern of exchange at pH 8.4 (see Figure 3C, E and 3D, F) and pH 9.0 (Supplementary Figure S2), in terms of the most and least protected regions was similar to that obtained for filaments, marked by a relatively strong protection of coil 1B and the C–terminal region of coil 2B in K8 and several short stable regions in K18 at positions 100, 205, and 330. Also, the fully flexible regions, the segments covering the head, tail, and linker L12 were the same under both conditions. For a detailed analysis of the differences between K8/K18 filaments and tetramers, one needs to compare the HDX patterns collected at different pH values (namely 7.5 *vs.* 8.4). It has been shown (Hvidt and Nielsen, 1966) that the observed rate constant of exchange k_{obs} depends on the structural factors and the intrinsic rate of exchange in unstructured peptide, and can be calculated according to the formula:

$$k_{obs} = k_{op} \cdot k_{int}/(k_{cl}+k_{int}) \qquad (1)$$

where:

k_{op} – rate constant for opening the structure to the exchange–competent state;
k_{cl} – rate constant for closing to the exchange-incompetent state
k_{int} – intrinsic rate constant of amide protons in the unstructured peptide.

Since k_{int} at neutral pH depends in a linear way on the concentration of [OD$^-$] ions, its pH dependence of k_{int} needs to be accounted for in comparisons of the experiments carried out at different pH values.

To further simplify the formula, the two kinetic limits EX1, and EX2 can be considered. In the EX1 limit, k_{cl} is assumed to be $<<k_{int}$, with each opening event leading to the full exchange. In this case, we obtain $k_{obs} = k_{op}$. Because k_{obs} in the EX1 limit become independent of k_{int}, no compensation is required, and a direct comparison of results obtained at different pH reveals the structural differences (namely changes in k_{op}). For keratins, this is illustrated by the differential plots, in which the difference in fraction exchanged in tetramer–promoting and filament–promoting conditions is shown (Figure 4A, B). It reveals difference in levels of exchange in several regions in K8, including N–terminal coil 1A, the coil2A–L2–coil2B interface, and coil 1B, 2B C–termini, while in K18 the differences encompass the center of coil 1B.

If the condition $k_{cl}<<k_{int}$ is not fulfilled, however, the pH dependence of k_{int} needs to be included in the analysis. For increasing k_{cl} values, a second kinetic EX2 limit can be

considered, as for $k_{cl}>>k_{int}$ formula (1) becomes simplified to $k_{obs} = k_{int}\cdot k_{op}/k_{cl}$. In the EX2 limit, the dependence of k_{obs} on k_{int} is thus linear. In this case, extraction of the changes in the structural component (k_{op}/k_{cl}) from experiments carried out at two pH values requires in this case the compensation for linear changes in k_{int} caused by the differences in [OD$^-$] ion concentration. We achieved this compensation by comparing the HDX patterns collected at different times of incubation. For instance, at pH 7.5, the [OD$^-$] ion concentration (and k_{int}) is 8–fold lower than at pH 8.4, so a 10 s incubation time at pH 8.4 should be compared with an 80 s incubation time for pH 7.5, to compensate for the difference in k_{int}. Figure 4C,D shows the results of the comparison of HDX patterns for K8 (C) and K18 (D) at pH 7.5 (80 s) and pH 8.4 (10 s) in the form of subtraction plots. In several regions, the strong differences observed in the direct comparison (Figure 4A, B) become less pronounced but are still statistically significant, namely N–terminal coil 1A, coil 2B center, and C–terminal coil 2B. Between the two extremes of the EX1 and EX2 regimes k_{cl} increases, as does the denominator in formula (1). Thus, k_{obs} values change in a monotonic fashion between the two extreme values. Therefore, independent of the exchange regime, obtained data indicate the stabilization of these three regions in filaments. There are also regions in which changes observed in Figure 4A,B disappear (coil 1B in K18) or change sign as in the coil 2A–L2 region, so the character of changes depends on the exchange regime in these regions.

A closer inspection of the MS spectra obtained for N–terminal coil 1A peptides during the exchange revealed that the signals in this coil 1A region were split into two groups corresponding to two distinct structural forms. As illustrated in two peptides from K8, V_{87}–F_{105} and K_{92}–F_{105} (Supplementary Figure S3, S3a), the splits were observed both for filaments at pH 7.5 (panels ii and iii) and for tetramers at pH 8.4, and 9.0 (panels iv and v). These peptides have also been marked “95.5” and “98”, respectively, in Figure 3A. In these peptides, upon incubation, the relative population of the protected form, marked “X,” decreases, with only a slight shift in the mass centers (compare panels iii and iv). This behavior indicates the domination of an EX1 mechanism of exchange caused by rapid global transitions from the folded state to a fully unfolded state of the N–terminal coil 1A. Such unfolding event leads to an instantaneous exchange in the region, without populating the intermediate exchange states. Although rather an exception than a rule, similarly clear–cut split regions were detected for N–terminal coil 2B peptides in K8 region 282–317 (Supplementary Figure S4 and Figure 5A), or coil 2B peptide (Figure 5B) and coil 1B peptide (Supplementary Figure S5) in K18. The exchange pattern in these regions was characterized by a gradual decay of the fraction of protected form “X”, following a prolonged incubation, implying EX1 mechanism and validity of the assumption $k_{cl} << k_{int}$. Therefore, the analysis carried out under this assumption (shown in Figure 4A, B) applies. This indicates that the stabilization observed in several regions, especially at the coil 1A N–terminus, on transition from tetramers to filaments is substantial.

Overall, the analysis of the exchange pattern differences between filaments and tetramers revealed stabilization of a few well–defined regions which included N–terminal coil 1A, coil 2B centre and the C–terminus of coil 2B. These segments are juxtaposed in models describing the elongation process of ULFs to filaments. Furthermore, a complex pattern of structural splits of the HROs was detected in selected regions. This finding underscores a high level of dynamics that is retained even in filaments.

3.5. Properties without a partner: HDX–MS of HMOs reveals coexistence of two structural forms

Filament formation is a multi–step process that obligatorily starts from monomers and, therefore, the structural properties of HMO preparations are also of interest to understand the assembly process. Moreover, it is not known how the cell handles the coiled–coil forming partners after translation. Hence, knowledge of their intrinsic properties and their behavior in the absence of the obligate coiled–coil complex partner molecule is important.

We observed in our AUC experiments that keratin HMOs formed large aggregates in both K8 and K18 at pH 7.5, predominantly dimers (K8) and monomers (K18) at pH 8.4 (data not shown), while at pH 9.0 a strong prevalence of dimers (K8) and monomers (K18) was observed (Table 1). However, the pre-concentration step necessary to carry out HDX experiments caused a strong decrease in the fraction of low s-value species (monomers for K18 and dimers for K8) observed after dilution. Instead, high order oligomeric forms prevailed, stabilized most probably by weak non-specific interactions.

Deuteration levels in HMOs of K8 and K18 were measured at different pH values, but further analysis is carried out using the data obtained at pH 9.0, since at higher pH the fraction of higher-sedimenting species was the lowest. Figures 6A and 6B show the results for K8 and K18, respectively. The most prominent feature of HDX in HMOs (also observed for lower pH preparations) was the presence of numerous regions with split isotopic envelopes. Different colors mark peptides representing each of these two forms. Again, strong splits indicated large differences in protection between the two structural states into which the HMOs were partitioned. All split peptides assigned to the unfolded form “Y” were poorly protected, indicating complete unfolding of many regions during frequent unfolding events.

Of interest, the very N–terminal peptides of the head domain, deprived of stable H–bonded structures in HROs, exhibited split isotopic envelopes in HMOs (Figure 7A, B: peptides S_2–S_{22} in K8 and S_2–Y_{13} in K18, marked “11.5” and “6.5”, respectively, in Figure 6). This feature implied the presence of a somehow structured N–terminal head region in the folded form “X” of both keratin HMOs. We also detected a second region in the head domain of K18 (positions S_{30}–R_{55}), which showed the same behavior. In HMOs, some regions of the head domain were engaged in a network of H–bonded interactions stabilizing the “structured” form. These structured head segments were absent from HROs as well as from the unfolded form “Y” of HMOs.

There also were several structured regions in HMOs in which the split is absent, such as the well–protected C–terminal regions of coils 1B and coil 2B. These regions retained a well–defined structure in the transition from “structured” form “X” into the “unstructured” form “Y”. HMOs undergo folding–unfolding transitions, but only in restricted regions, the other regions are either stable or fully flexible. Figure 8 illustrates the placement of structured and unstructured regions in both forms.

The presence of massive splits and specific H-bonding networks in HMOs, which are absent in HROs, could in principle be attributed to the prevalence of higher order aggregates in HMOs. However, in HROs 20-30% higher order oligomers are also present but splits in many regions, and H-bonding networks in the head region are completely absent. So we find the possibility that weak non-specific interactions might be responsible for the observed well localized and HMO-specific patterns of H-bonding unlikely.

3.6. Levels of structural stability varied markedly along the sequence in the folded form of HMOs

In the structured form “X” of HMOs of both keratins at either pH, the head region can be divided into sub–regions: either structured (N–terminal and the one centered at position 45 in K18) or unstructured. The unfolded region extended from the C–terminus of the head region to the N–terminal half of coil 1A. These data corresponds well to the speculative view presented for the corresponding segment in vimentins based on the behavior of the corresponding synthetic peptide representing coil 1A (Strelkov et al., 2002a). In general, in

HMOs even in their structured form, the relatively stable regions are much shorter that in HROs, separated by longer unstable regions, also covering central parts of coils 1B and 2B. In K8, the coil 2B flexible region was longer and covered a central part of the coil, whereas, in K18 it was shifted towards the N–terminus of this coil. The fully exposed central region of coil 2B in K8 encompassed the stutter region (G_{342} marked by the arrow in Figure 6A). The stutter region represents a disruption of the heptad repeat patterns in the middle of coil 2B (Strelkov et al., 2003) by introducing a hendecad repeat. This region is highly conserved among all IF proteins (Herrmann and Aebi, 2004), and from atomic structures obtained by X–ray crystallography of vimentin, K5/14 heterodimer, and lamin A, it became apparent that the stutter region represented two α–helical segments in parallel, also referred to as a "paired bundle" (Herrmann et al., 2007; Strelkov et al., 2002b). Substantial protection was shown by the peptides covering the stutter region in K18 (at Y_{331}; Figure 6B).

Evidence of structure formation of head and tail segments only in HMO indicates that these segments interact with elements of the exposed coiled–coils in the absence of their proper partner. This interaction leads to stabilization of coiled–coils, as observed in the "structured" form of HMOs. Such pre–forming stabilization of α–helical segments along a monomer might be advantageous by means of increasing the number of productive encounters of monomers on the way to HRO formation.

For K18 HMOs at pH 9.0, the presence of split isotopic envelopes indicated the presence of the structured form, with unfolding events restricted to selected regions in different parts of the molecule. We suggest that the highly charged, mostly intrinsically disordered head and tail domains fold back in the absence of significant amounts of monovalent ions, onto the highly charged rod domain. This folding probably causes a considerable stabilization of the "structured" monomer. Correspondingly, an interaction of the tail domain with the rod has been demonstrated for type III IF proteins by immunological means (Kouklis et al., 1991).

For K8 HMOs at pH 9.0, where dimeric species predominate, we observed that the isotopic splits and unfolding were restricted to the N–terminal half, around position 282. Thus, monomers in the dimeric forms contact only *via* equally well–protected, short structured regions (coils 1B, 2B termini). In the "structured" form, the engagement of head peptides led to the stabilization of other regions of the coil segments.

The overall characteristic patterns of exchange for structured forms in HMOs were highlighted by a few well–defined strongly protected regions. In particular, this feature was revealed for regions at the C–termini of coils 1B and coil 2B. These regions were stable in both the structured and unstructured form for both proteins. In contrast, N–terminal regions of these coils were relatively stable only in the structured form. Unlike in the heterocomplex, there was a substantial segment of instability in the center of coil 1B of K8, less pronounced for K18. Moreover, much more pronounced regions of relative instability were discovered in coil 2B of both proteins. Also, the HMO–specific involvement of distinct head segments (K8 and K18) and tail segments (K18) in the stabilization of the structured forms of HMOs is noteworthy.

3.7. A strong structural difference between oligomeric HMOs and HROs

The differences between the exchange patterns in HMOs and HROs were visualized as differential plots (Figure 9A,B) obtained by subtracting the fraction exchanged in HRO (tetramers, pH 8.4) from that of the folded forms of HMO at pH 8.4. We observed an overall strong stabilization of the coiled–coil rod regions in HROs, as compared to HMOs. The strongest increases in stability for K8 were concentrated in the head–coil 1A interface and the centers of coils 1B and 2B. For K18, the stabilization effect was not as strong and was more evenly distributed across the entire rod region. The main difference between HMO and HRO forms was mainly the absence of internal regions of instability within coiled–coil segments. This observation agreed with the fact that HROs, formed from one acidic and one basic keratin, are the native form found in keratin intermediate filaments. Thus, HROs are expected to be more stable than corresponding HMOs.

In contrast, we also observed regions that became less structured in HROs as compared to HMOs. The most prominent of these regions included two head segments and a large part of the tail in K18. In K18, both head and tail participated in the intramolecular stabilization of the coiled-coils. Head segments in K8 formed a network of interactions, most probably with the coiled–coil region of the dimer. Furthermore, two additional regions were found to be destabilized in HROs. For K8, this was a segment denoted as 313, and for K18, it was denoted as 277 (I_{275}–T_{280}), both in the N–terminal part of coils 2B (Figure 5A, B). The instability in the internal region of coil 2B, observed in HMOs, shifted towards the N–terminus of coil 2B in HROs, thus exposing these segments. This observation accounts for the phenomenon of the HRO–specific affinity of an antibody directed to a region surrounding position 313 in K8 (Waseem et al., 2004).

3.8. From monomers to dimers to tetramers to filaments

The formation of keratin filaments from individual monomers to dimers, tetramers, and ULFs is a multi–stage process involving well–defined patterns of interactions at each stage of assembly. Our model study on HMOs suggests a possible scenario for this assembly. Participation of the head and/or tail domains in the intramolecular interactions with preformed coiled–coil segments helps to stabilize them in monomers and dimers. When these low–order structures combine to form a K8/K18 HRO, the head, and tail interactions are replaced by intermolecular interactions of coiled coils. In the next step N–termini of coil 1A, C–termini and central segments of coil 2B become stabilized by the formation of an increased network of contacts within the filaments.

4. Discussion

In the work presented here, we employed HDX–MS to obtain insights into the structural properties of functional keratin K8 and K18 complexes at a medium–resolution level. Therefore, we have mapped the hydrogen–deuterium exchange of amide protons of K8 and K18 complexes at different pH values, i.e. pH 9.0, pH 8.4 and pH 7.5. The rationale for choosing these conditions was that keratins correspondingly adopt distinct structures ranging from tetramers to filaments. At the intermediate pH value, higher than tetrameric oligomers but no filaments yet are obtained (Table 1), indicating they are stalled for longitudinal annealing. Nevertheless, these complexes are true intermediates as during assembly by dialysis the tetramers necessarily transit this state on their way to filaments. In each case, we have localized regions characterized by varying levels of protection. Moreover, we have mapped structural signatures specific for heterodimers in their respective assembly complexes in comparison to oligomers formed by K8 and K18 alone to understand the genuine structural features of the productive dimeric building block.

4.1. A structural tetramer model for keratins K8 and K18

According to predictions from their primary amino acid sequences, the domain structure conservation in mammalian IF proteins is exceptionally high. Hence, the substructure of the central α–helical “rod” domain is partitioned into 35 amino acids to coil 1A, 101 to coil 1B, 19 to coil 2A and 121 to coil 2B (Parry D.A.D., 1995) (Fig. 1A; for details see(Conway and Parry, 1988)). These numbers are the same for all cytoplasmic IF proteins, keratins to neurofilament proteins and vimentin. Some little variation comes in with the “linker” domains L1, L12 and L2 connecting these four α–helical segments. Linkers L1 and L12 vary in length (~8 versus ~15 amino acids) and may contain amino acids not favorable for α–helix formation. L2 is always eight amino acids long; all amino acids are compatible with α–helix formation. Therefore, early on it was assumed that L2 together with coil 2A and coil 2B forms a continuous α–helix termed coil 2 (Herrmann et al., 2007). For vimentin, this concept has been verified by X–ray crystallography (Chernyatina et al., 2012). Hence, former coil 2A and L2 together with the first one and a half heptad of coil 2B form a “paired bundle” of two α–helices, constituted by three 11–residue (hendecad) repeats and a single *h* to *k* segment (see Figure 1 in (Herrmann and Aebi, 2004), and Figure1 in (Chernyatina et al., 2015)). The remainder of coil 2B is a coiled coil except for one hendecad segment near the center of coil 2B, which was formerly named “stutter”. Here again, the two α–helices run in parallel. This stutter is located at the very same position in all IF proteins (Strelkov et al., 2002). According to the high sequence identity of vimentin with keratins K8 and K18, we assume, in the absence of X–ray structure, that the keratins exhibit a corresponding structural organization in this part of the dimer (Figure 1C). Furthermore, keratin K8 and K18 form tetramers that behave identically to vimentin tetramers as determined by analytical ultracentrifugation. Their filament assembly proceeds also via longitudinal annealing of mini–filaments of the “unit–length” filament type (Herrmann et al., 2002; Lichtenstern et al., 2012).

4.2. Overall exchange dynamics in tetramers and filaments

After we had worked out a procedure to employ the HDX method for keratins, we were able to address the question if significant alterations in the exchange dynamics in distinct regions of the coiled coils take place between tetramers and filaments. Firstly, we observed increased dynamics in coil 2B as compared to coil 1B. Secondly, the dynamic character of the coil 2B N–terminus is largely retained in filaments. Thirdly, in filaments coil 1B of K8 shows slightly higher stability than coil 1B in K18 (Fig. 3A, B). Even though this finding seems counterintuitive at first thought – as both proteins interact in the form of a coiled coil, previous work has demonstrated that substantially variable exchange of amide proton at different sites within one and the same coiled coil may occur (Goodman and Kim, 1991). Last but not least, our data give experimental support to previous models of filament assembly. In the context of full-length, unmodified keratins we have now localized unique structural elements that undergo stabilization in the transition from tetramers to filaments, namely: N-terminus of coil 1A, coil 2B center and C–terminus. These three segments are assumed to be brought close to each other in the filament model.

4.3. Heads and tails

The importance of the head domain of IF proteins for assembly has been noted early on (Heins and Aebi, 1994). In particular, headless IF proteins do not form tetramers under tetramer assembly conditions indicating that the head domains mediate an interaction between neighboring coiled–coil dimers (Herrmann et al., 1996). This interaction is most likely achieved by ionic interactions of the basic arginine residues and the acidic patches on the rod domain. Note that the vimentin head contains 12 arginines and that the rod exhibits 24 acid residues in excess of basic ones. Moreover, the spatial distribution of basic and acidic residues in the rod is evolutionarily conserved. Thus, Parry and Conway assumed that this striking regularity in the homology distribution of the ionic residues of the major classes of IF proteins in functional terms emerged "... probably as a consequence of its importance in specifying the aggregation of molecules in IF" (Conway and Parry, 1988). A comparison of the amino acid sequences of keratin K8 and K18 reveals that the charge properties are very similar to those of vimentin.

Our study shows that both in tetramers and filaments, no H–bonded networks are present in the head domains. This finding is in agreement with their previously suggested overall structural flexibility and lack of structure (Omary et al., 2006). On the other hand, the head domain is essential for directing alignment of dimers, stabilization of tetramers, and elongation and assembly of IFs (Hatzfeld and Burba, 1994; Hatzfeld et al., 1987; Herrmann and Aebi, 2004). The direct involvement of the head region in stabilizing the tetramer complex can be rationalized by the formation of a network of ionic interactions involving the multiple arginines without accompanying H–bonding networks. Glycine loop motifs of the form XaaGly$_n$, where Xaa stands mainly for aromatic residues with less frequent long aliphatic chains. These have previously been suggested to induce structural ordering into IF protein head domains (Parry and Steinert, 1995; Herrmann and Aebi, 1998a). Also, salt bridges involving basic residues from the head domain are essential for tetramer formation in K8/K18 and IF assembly (Herrmann et al., 2009). The tails are not needed for the formation of tetramers (Herrmann et al., 1996; Mücke et al., 2004).

Our data show, however, that some segments in the head domains of K8 and K18 as well as in the tail domain of K18 can be structured through the participation of an H–bonded network, but only when keratins are deprived of their native partners, i.e. in homomeric preparations in which keratins do not form specific oligomers larger than monomers (K18) or dimers (K8). In these forms structurally well–defined H–bonded head segments are prominent whereas they are absent in tetramers and filaments. Of interest, structured segments of heads correlate with clusters of positively charged residues. In K8, seven out of nine and in K18 five out of six of the basic head residues (arginine or lysine) are localized within structured segments. In contrast, glycine loop clusters (in K8 at F_{46}–M_{60} and in K18 at G_{56}–Q_{78}) lie outside these segments. Our results suggest that the intra–molecular interactions within segments of the head allow maintaining, even at the level of monomers, an α–helical structure of coil 1B, which is a core stabilizing unit of the tetramer. Additionally, the tail region, which has no decisive role in IF assembly *in vitro*, is engaged in stabilizing the residual structure of the K18 itself, most probably in the coil 2B region. However, previous reports showed that tailless keratins still retain the ability to form IFs *de novo* (Bader et al., 1991; Hatzfeld and Weber, 1990a; Hatzfeld et al., 1987). Coil 2B–tail contacts detected in our work in K18 may be dispensable because it is coil 1B that is crucial in construction of higher order oligomeric forms, due to the staggered nature of coil 2B in tetramers and ULFs. In conclusion, our results point to a different or alternative role for head/tail regions that may be necessary to pre–form helical segments of coiled-coils *via* intra–molecular contacts and facilitate proper intermolecular coiled–coil pairing. At the tetramer stage, head and tail make other types of contacts. Indeed, it is assumed that during renaturation, the head domains are stalled through strong interactions of the head arginines with the rod. This view is supported by the fact that keratins K8 and K18, kept at 2 mM Tris–HCl, pH 9.0, will explosively form huge filamentous networks, when 23–mer "head"–peptides, are added in micromolar concentration (Herrmann et al., 2002). This effect is strongly enhanced when the peptides are added in a dimeric form, as obtained by cysteine crosslinking at the C–terminal end. Thus, keratin filaments do massively form at "non–assembly" conditions, as soon as the heads are freed from their blocked status by the competitive interaction of the peptides.

4.4. The coiled–coil subdomains

The α–helical coiled–coil regions are the main anchoring segments directing the assembly of keratins into filaments (Hatzfeld and Weber, 1990b). Specific regions of coil 1B and coil 2B are thought to be indispensable for stability for α–helical IF rods (Bragulla and Homberger, 2009). In the case of the K5/K14 keratin pair, these regions contained two coiled–coil trigger motifs, one in coil 1B, and the other in coil 2B (Wu et al., 2000). Our data identified regions in K8 and K18, in which H–bonding networks are equally strong in all studied forms, from the unstable form of monomer in K18 to the heteromeric filament. These networks include the coil 1B region R_{225}–L_{235} in K8 and E_{200}–L_{210} in K18, and the coil 2B region E_{355}–T_{390} in K8 and R_{325}–F_{390} in K18. The last two directly precede the strictly conserved IF consensus motif YRKLLEGEE, which is critical for correct filament assembly (Herrmann and Aebi, 1998b; Herrmann et al., 2000). These K8/K18 HDX–stable regions exactly match in sequence alignment the above–mentioned K5/K14 trigger motifs.

In K8, the strong protection of coil 1B covers its center in HROs but not in HMOs, indicating the substantial flexibility of coil 1B in the HMO structure. In analogy, the motion of EPR spin probes located in the homodimeric vimentin central coil 1B residues A_{169}–M_{193} (corresponding to residues L_{159}–I_{183} in K8) was found to vary from moderate to strong despite well–defined intermolecular contacts (Hess et al., 2004). Such relative flexibility at the center of coil 1B, indicated by the EPR study, was found here to be much more prominent in the case of K8 and K18 HMOs than HROs. EPR probes localized at the coil 2B N–terminus of vimentin showed restricted motion and intermolecular contacts (Hess et al., 2002), indicating a coiled–coil structure in this region as corroborated for vimentin by X–ray crystallization. This region in our study showed the relatively weakest protection as compared to other parts of coil 2B. However, the level of protection in the N–terminal coil 2B is still significantly higher than in fully exposed regions, like head or tail, indicating entangled H–bonding in this region.

At the C–terminal part of coil 2B, the region of structural stability in filaments is shifted from its C–terminus, especially in K18, whereas the C–terminus itself remains only partly protected (Figure 3). This fragment contains the YRKLLEGEE IF–conserved sequence serving most probably as a helix–termination signal (Wu et al., 2000). In general, the coiled–coil region is mostly stabilized upon transition from monomers/dimers to tetramers (Figure 9) because of expansion of the stable regions from the termini of coils 1B and 2B towards their central segments. The N–terminal part of coil 2B (both proteins) is an exception, as it retains relative flexibility even in filaments (Figure 3A, B). This region may be responsible for IF flexibility because IFs *in vivo* are known to be highly dynamic structures (Strelkov et al., 2003). It is also known that the interaction with protein partners requires some rearrangements of the IF structure (Herrmann and Aebi, 2000) and even subunit exchange can be observed. Such flexibility is absent in actin microfilaments and tubulin microtubules but might be important functionally in IFs. In this context, single molecule studies carried out with vimentin coil 2B are striking. It has been demonstrated that forces needed to pull the coiled–coil structure apart is lower at the N–terminal and significantly higher in the C–terminal part (Ramm et al., 2014)**.**

Our experiments provided peptide–specific information about the structural stability of different protein subdomains with good sequence coverage along the protein sequence. These data correlated well with known structural properties of keratins and elucidated new features: 1) strict compartmentalization of coil 2B into relatively protected C–terminal and relatively exposed N–terminal regions, revealing the molecular basis of keratin flexibility; 2) indication of a folded–unfolded equilibrium in sequence regions (coil 1A), affecting not only tetramers but also filaments; and 3) identification of regions of different exchange patterns upon transition from tetramers to filaments. Of note, the highly conserved ends of the α–helical rod domains, representing the "IF consensus motifs" are stabilized by formation of IFs. This stabilization is probably the result of their direct and strong physical interaction in the course of the "head–to–tail" overlap formation that mediates elongation (Kapinos et al., 2010).

4.5. Conclusions

Our work presented here provides an analytical platform for further studies in which different types or variants of keratins, truncated or mutated, could be explored to advance our understanding of the intra– and intermolecular interactions, directing various phases of the complex transitions from monomers to filaments. In this way, further insight can be obtained into the structural changes relevant for the mechanism of keratin IF assembly.

Acknowledgements

We kindly acknowledge financial support from the Foundation for Polish Science TEAM/2011–7/1, EU CEPT (POIG.02.02.00–14–024/08–00) and NanoFun (POIGT.02.02.00–00–025/09–00) Program. HH received support from the German Research Foundation (DFG, HE1853/11–1).

We also thank Dr. Roman Szczepanowski, Core Biophysical Facility, International Institute of Molecular and Cell Biology, for his valuable expertise and advice in the interpretation and understanding of Analytical Ultracentrifugation data.

*To whom correspondence may be addressed: Institute of Biochemistry and Biophysics, Department of Biophysics, 02–106 Warsaw, Tel.: +48 22 5923 471; fax: +48 22 658 4766; michald@ibb.waw.pl

References

Aziz, A., Hess, J.F., Budamagunta, M.S., Voss, J.C., Kuzin, A.P., Huang, Y.J., Xiao, R., Montelione, G.T., FitzGerald, P.G., Hunt, J.F., 2012. The structure of vimentin linker 1 and rod 1B domains characterized by site-directed spin-labeling electron paramagnetic resonance (SDSL-EPR) and X-ray crystallography. J. Biol. Chem. 287, 28349–61.

Bader, B.L., Magin, T.M., Freudenmann, M., Stumpp, S., Franke, W.W., 1991. Intermediate filaments formed de novo from tail-less cytokeratins in the cytoplasm and in the nucleus. J. Cell Biol. 115, 1293–307.

Bou-Assaf, G.M., Chamoun, J.E., Emmett, M.R., Fajer, P.G., Marshall, A.G., 2011. Complexation and Calcium-Induced Conformational Changes in the Cardiac Troponin Complex Monitored by Hydrogen/Deuterium Exchange and FT-ICR Mass Spectrometry. Int. J. Mass Spectrom. 302, 116–124.

Bragulla, H.H., Homberger, D.G., 2009. Structure and functions of keratin proteins in simple, stratified, keratinized and cornified epithelia. J. Anat. 214, 516–59.

Chernyatina, A.A., Guzenko, D., Strelkov, S. V, 2015. Intermediate filament structure: the bottom-up approach. Curr. Opin. Cell Biol. 32, 65–72.

Chernyatina, A.A., Nicolet, S., Aebi, U., Herrmann, H., Strelkov, S. V, 2012. Atomic structure of the vimentin central α-helical domain and its implications for intermediate filament assembly. Proc. Natl. Acad. Sci. U. S. A. 109, 13620–5.

Conway, J.F., Parry, D.A.D., 1988. Intermediate filament structure: 3. Analysis of sequence homologies. Int. J. Biol. Macromol. 10, 79–98.

Coulombe, P.A., Fuchs, E., 1990. Elucidating the early stages of keratin filament assembly. J. Cell Biol. 111, 153–69.

Eichner, R., Rew, P., Engel, A., Aebi, U., 1985. Human Epidermal Keratin Filaments: Studies on Their Structure and Assembly. Ann. N. Y. Acad. Sci. 455, 381–402.

Franke, W. W., Schiller, D. L. & Grund, C., 1982. Protofilamentous and annular structures as inter- mediates during reconstitution of cytokeratin filaments in vitro. Biol. Cell. 46, 257–268.

Goodman, E.M., Kim, P.S., 1991. Periodicity of amide proton exchange rates in a coiled-coil leucine zipper peptide. Biochemistry 30, 11615–11620.

Guldiken, N., Usachov, V., Levada, K., Trautwein, C., Ziol, M., Nahon, P., Strnad, P., 2015. Keratins 8 and 18 are type II acute-phase responsive genes overexpressed in human liver disease. Liver Int. 35, 1203–12.

Guttman, M., Weis, D.D., Engen, J.R., Lee, K.K., 2013. Analysis of overlapped and noisy hydrogen/deuterium exchange mass spectra. J. Am. Soc. Mass Spectrom. 24, 1906–12.

Hatzfeld, M., Burba, M., 1994. Function of type I and type II keratin head domains: their role in dimer, tetramer and filament formation. J. Cell Sci. 107 (Pt 7, 1959–72.

Hatzfeld, M., Franke, W.W., 1985. Pair formation and promiscuity of cytokeratins: formation in vitro of heterotypic complexes and intermediate-sized filaments by homologous and heterologous recombinations of purified polypeptides. J. Cell Biol. 101, 1826–41.

Hatzfeld, M., Maier, G., Franke, W.W., 1987. Cytokeratin domains involved in heterotypic complex formation determined by in-vitro binding assays. J. Mol. Biol. 197, 237–55.

Hatzfeld, M., Weber, K., 1990a. Tailless keratins assemble into regular intermediate filaments in vitro. J. Cell Sci. 97 (Pt 2), 317–24.

Hatzfeld, M., Weber, K., 1990b. The coiled coil of in vitro assembled keratin filaments is a heterodimer of type I and II keratins: use of site-specific mutagenesis and recombinant protein expression. J. Cell Biol. 110, 1199–210.

Heins, S., Aebi, U., 1994. Making heads and tails of intermediate filament assembly, dynamics and networks. Curr. Opin. Cell Biol. 6, 25–33.

Herrmann, H., Aebi, U., 2004. Intermediate filaments: molecular structure, assembly mechanism, and integration into functionally distinct intracellular Scaffolds. Annu. Rev. Biochem. 73, 749–89.

Herrmann, H., Aebi, U., 2000. Intermediate filaments and their associates: multi-talented structural elements specifying cytoarchitecture and cytodynamics. Curr. Opin. Cell Biol. 12, 79–90.

Herrmann, H., Aebi, U., 1998a. Structure, assembly, and dynamics of intermediate filaments. Subcell. Biochem. 31, 319–62.

Herrmann, H., Aebi, U., 1998b. Intermediate filament assembly: fibrillogenesis is driven by decisive dimer-dimer interactions. Curr. Opin. Struct. Biol. 8, 177–85.

Herrmann, H., Bär, H., Kreplak, L., Strelkov, S. V, Aebi, U., 2007. Intermediate filaments: from cell architecture to nanomechanics. Nat. Rev. Mol. Cell Biol. 8, 562–73.

Herrmann, H., Häner, M., Brettel, M., Müller, S.A., Goldie, K.N., Fedtke, B., Lustig, A., Franke, W.W., Aebi, U., 1996. Structure and assembly properties of the intermediate filament protein vimentin: the role of its head, rod and tail domains. J. Mol. Biol. 264, 933–53.

Herrmann, H., Hofmann, I., Franke, W.W., 1992. Identification of a nonapeptide motif in the vimentin head domain involved in intermediate filament assembly. J. Mol. Biol. 223, 637–50.

Herrmann, H., Kreplak, L., Aebi, U., 2004a. Isolation, characterization, and in vitro assembly of intermediate filaments. Methods Cell Biol. 78, 3–24.

Herrmann, H., Kreplak, L., Aebi, U., 2004b. Intermediate Filament Cytoskeleton, Methods in Cell Biology, Methods in Cell Biology. Elsevier.

Herrmann, H., Strelkov, S. V, Burkhard, P., Aebi, U., 2009. Intermediate filaments: primary determinants of cell architecture and plasticity. J. Clin. Invest. 119, 1772–83.

Herrmann, H., Wedig, T., Porter, R.M., Lane, E.B., Aebi, U., 2002. Characterization of early assembly intermediates of recombinant human keratins. J. Struct. Biol. 137, 82–96.

Hess, J.F., Budamagunta, M.S., Voss, J.C., FitzGerald, P.G., 2004. Structural characterization of human vimentin rod 1 and the sequencing of assembly steps in intermediate filament formation in vitro using site-directed spin labeling and electron paramagnetic resonance. J. Biol. Chem. 279, 44841–6.

Hess, J.F., Voss, J.C., FitzGerald, P.G., 2002. Real-time observation of coiled-coil domains and subunit assembly in intermediate filaments. J. Biol. Chem. 277, 35516–22.

Hofmann, I., Winter, H., Mücke, N., Langowski, J., Schweizer, J., 2002. The in vitro assembly of hair follicle keratins: comparison of cortex and companion layer keratins. Biol. Chem. 383, 1373–81.

Hvidt, A., Nielsen, S.O., 1966. Hydrogen exchange in proteins. Adv. Protein Chem. 21, 287–386.

Kacprzyk-Stokowiec, A., Kulma, M., Traczyk, G., Kwiatkowska, K., Sobota, A., Dadlez, M., 2014. Crucial role of perfringolysin O D1 domain in orchestrating structural transitions leading to membrane-perforating pores: a hydrogen-deuterium exchange study. J. Biol. Chem. 289, 28738–52.

Kapinos, L.E., Schumacher, J., Mücke, N., Machaidze, G., Burkhard, P., Aebi, U., Strelkov, S. V, Herrmann, H., 2010. Characterization of the head-to-tail overlap complexes formed by human lamin A, B1 and B2 “half-minilamin” dimers. J. Mol. Biol. 396, 719–31.

Kayser, J., Haslbeck, M., Dempfle, L., Krause, M., Grashoff, C., Buchner, J., Herrmann, H., Bausch, A.R., 2013. The small heat shock protein Hsp27 affects assembly dynamics and structure of keratin intermediate filament networks. Biophys. J. 105, 1778–85.

Kouklis, P.D., Papamarcaki, T., Merdes, A., Georgatos, S.D., 1991. A potential role for the COOH-terminal domain in the lateral packing of type III intermediate filaments. J. Cell Biol. 114, 773–86.

Lichtenstern, T., Mücke, N., Aebi, U., Mauermann, M., Herrmann, H., 2012. Complex formation and kinetics of filament assembly exhibited by the simple epithelial keratins K8 and K18. J. Struct. Biol. 177, 54–62.

Lieleg, O., Kayser, J., Brambilla, G., Cipelletti, L., Bausch, A.R., 2011. Slow dynamics and internal stress relaxation in bundled cytoskeletal networks. Nat. Mater. 10, 236–42.

Marcsisin, S.R., Engen, J.R., 2010. Hydrogen exchange mass spectrometry: what is it and what can it tell us? Anal. Bioanal. Chem. 397, 967–972.

Marsh, J.J., Guan, H.S., Li, S., Chiles, P.G., Tran, D., Morris, T.A., 2013. Structural insights into fibrinogen dynamics using amide hydrogen/deuterium exchange mass spectrometry. Biochemistry 52, 5491–502.

Meier, M., Padilla, G.P., Herrmann, H., Wedig, T., Hergt, M., Patel, T.R., Stetefeld, J., Aebi, U., Burkhard, P., 2009. Vimentin coil 1A-A molecular switch involved in the initiation of filament elongation. J. Mol. Biol. 390, 245–61.

Moll, R., Divo, M., Langbein, L., 2008. The human keratins: biology and pathology. Histochem. Cell Biol. 129, 705–33.

Mücke, N., Kreplak, L., Kirmse, R., Wedig, T., Herrmann, H., Aebi, U., Langowski, J., 2004. Assessing the flexibility of intermediate filaments by atomic force microscopy. J. Mol. Biol. 335, 1241–50.

Nagai, K., Thøgersen, H.C., 1987. Synthesis and sequence-specific proteolysis of hybrid proteins produced in Escherichia coli. Methods Enzymol. 153, 461–81.

Nicolet, S., Herrmann, H., Aebi, U., Strelkov, S. V, 2010. Atomic structure of vimentin coil 2. J. Struct. Biol. 170, 369–76.

Odolczyk, N., Fritsch, J., Norez, C., Servel, N., da Cunha, M.F., Bitam, S., Kupniewska, A., Wiszniewski, L., Colas, J., Tarnowski, K., Tondelier, D., Roldan, A., Saussereau, E.L., Melin-Heschel, P., Wieczorek, G., Lukacs, G.L., Dadlez, M., Faure, G., Herrmann, H., Ollero, M., Becq, F., Zielenkiewicz, P., Edelman, A., 2013. Discovery of novel potent ΔF508-CFTR correctors that target the nucleotide binding domain. EMBO Mol. Med. 5, 1484–501.

Omary, M.B., Ku, N.-O., Strnad, P., Hanada, S., 2009. Toward unraveling the complexity of simple epithelial keratins in human disease. J. Clin. Invest. 119, 1794–805.

Omary, M.B., Ku, N.-O., Tao, G.-Z., Toivola, D.M., Liao, J., 2006. “Heads and tails” of intermediate filament phosphorylation: multiple sites and functional insights. Trends Biochem. Sci. 31, 383–94.

Parry, D., Steinert, P., 1999. Intermediate filaments: molecular architecture, assembly, dynamics and polymorphism. Q. Rev. Biophys. 32, 99–187.

Parry, D.A.D., 2005. Microdissection of the sequence and structure of intermediate filament chains. Adv. Protein Chem. 70, 113–42.

Parry D.A.D., S.P.M., 1995. The Structure and Function of Intermediate Filaments, E. Landis Publishing Company. Austin, TX.

Parry, D.A.D., Strelkov, S. V, Burkhard, P., Aebi, U., Herrmann, H., 2007. Towards a molecular description of intermediate filament structure and assembly. Exp. Cell Res. 313, 2204–16.

Philo, J.S., 2006. Improved methods for fitting sedimentation coefficient distributions derived by time-derivative techniques. Anal. Biochem. 354, 238–46.

Ramm, B., Stigler, J., Hinczewski, M., Thirumalai, D., Herrmann, H., Woehlke, G., Rief, M., 2014. Sequence-resolved free energy profiles of stress-bearing vimentin intermediate filaments. Proc. Natl. Acad. Sci. 111, 11359–11364.

Stafford, W.F., 1992. Boundary analysis in sedimentation transport experiments: A procedure for obtaining sedimentation coefficient distributions using the time derivative of the concentration profile. Anal. Biochem. 203, 295–301.

Strelkov, S. V, Herrmann, H., Aebi, U., 2003. Molecular architecture of intermediate filaments. Bioessays 25, 243–51.

Strelkov, S. V, Herrmann, H., Geisler, N., Wedig, T., Zimbelmann, R., Aebi, U., Burkhard, P., 2002a. Conserved segments 1A and 2B of the intermediate filament dimer: their atomic structures and role in filament assembly. EMBO J. 21, 1255–1266.

Strelkov, S. V, Herrmann, H., Geisler, N., Wedig, T., Zimbelmann, R., Aebi, U., Burkhard, P., 2002b. Conserved segments 1A and 2B of the intermediate filament dimer: their atomic structures and role in filament assembly. EMBO J. 21, 1255–66.

Szeverenyi, I., Cassidy, A.J., Chung, C.W., Lee, B.T.K., Common, J.E.A., Ogg, S.C., Chen, H., Sim, S.Y., Goh, W.L.P., Ng, K.W., Simpson, J.A., Chee, L.L., Eng, G.H., Li, B., Lunny, D.P., Chuon, D., Venkatesh, A., Khoo, K.H., McLean, W.H.I., Lim, Y.P., Lane, E.B., 2008. The Human Intermediate Filament Database: comprehensive information on a gene family involved in many human diseases. Hum. Mutat. 29, 351–60.

Wales, T.E., Engen, J.R., 2006. Hydrogen exchange mass spectrometry for the analysis of protein dynamics. Mass Spectrom. Rev. 25, 158–170.

Waseem, A., Karsten, U., Leigh, I.M., Purkis, P., Waseem, N.H., Lane, E.B., 2004. Conformational changes in the rod domain of human keratin 8 following heterotypic association with keratin 18 and its implication for filament stability. Biochemistry 43, 1283–95.

Wu, K.C., Bryan, J.T., Morasso, M.I., Jang, S.I., Lee, J.H., Yang, J.M., Marekov, L.N., Parry, D.A., Steinert, P.M., 2000. Coiled-coil trigger motifs in the 1B and 2B rod domain segments are required for the stability of keratin intermediate filaments. Mol. Biol. Cell 11, 3539–58.

FIGURE LEGENDS

Table 1. Analytical ultracentrifugation of K8 and K18: Determination of the association state of keratins K8, K18, and K8/K18 by sedimentation velocity ultracentrifugation.

Figure 1. A schematic representation of IF protein organization: (A) Traditional sub–domain classification based on computed α–helicity. These α–helical regions (boxed) were thought to form coiled–coils. Non–α–helical N–terminal (head) and C–terminal (tail) are represented as lines, as are linker L1 and L12. In contrast, L2 is considered to be α–helical and is represented by a striped box. Numbers above the boxes indicate the lengths of sub–domains conserved over IFs and across species. The blue areas in N–terminal coil 1A and C–terminal coil 2B represent evolutionarily highly conserved sequence elements. *Stu* indicates an irregularity in the heptad pattern, called a "stutter." (Conway and Parry, 1988) (B) Structure–derived molecular model of a coiled–coil dimer of keratin 8 (green) and keratin 18 (blue) highlighting the paired bundle (pb) and stutter (st) running as two parallel α–helices (yellow), as originally demonstrated for vimentin (Herrmann et al., 2007; Nicolet et al., 2010). (C) Sequence comparison in the paired bundle segment of K18, K8, and vimentin. "Repeat" indicates the extension of 7–residue (heptad) patterns into the 11–residue (hendecad) patterns. *a* and b in "Coil" indicates the regions that were formerly attributed to the older designation of coil 2A and 2B, respectively. Dashes were previously attributed to L2 segment (Herrmann and Aebi, 2004).

Figure 2. Transmission electron microscopy of negatively stained samples of different preparations of keratins: (A, C) keratin 8 at pH 8.4; (B, D) keratin 18 at pH 8.4, either without pre–concentration step (A, B) or with pre–concentration step (C, D).

Figure 3. Overview of exchange patterns of keratins K8 and K18 in HROs: fraction of exchange (% deuteration) of amide protons in peptides for filament– (A, B) and tetramer– (C, D) promoting conditions in keratin 8 (A, C, E) and keratin 18 (B, D, F). Coil domains are marked by gray rectangles. The peptide position in the sequence is shown on the horizontal axis represented by a horizontal bar of length equal to that of the peptide. The position of the bar at the vertical axis marks the fraction exchanged after 10 s of exchange. Values close to 100% indicate fully unprotected regions, i.e., regions of high flexibility, whereas values close to 0% represent protected regions, indicating a stable structure. Y–axis error bars are standard deviations calculated from three independent experiments. (E, F) Schematic representation of

the earlier depicted exchange pattern for K8 (E) and K18 (F) in filaments and tetramers. The average exchange level for a given substructure or its part in the folded form was color coded with dark blue indicating relatively well–protected regions (<20%); light blue, protected (20–40%); green, moderately protected (40–60%); light green, poorly protected (60–80%); red, fully unprotected; and white, gaps– regions not represented in MS analysis. Arrows point to the stutter region.

Figure 4. Exchange patterns differences between tetramers and filaments: Differences in the fraction of exchange for peptides of K8 (A, C) and K18 (B, D) in filaments and tetramers. The position of the bar on the vertical axis marks the result of subtraction of the fraction exchanged (in %) in tetramers (pH 8.4) after 10 sec of exchange with filaments (pH 7.5) after 10 s (A, B) and 80 s (C, D) of exchange (see text). Error bars are calculated as the square root of the sum of variation of the subtracted data points. Regions of interest are circled in red.

Figure 5. Isotopic envelopes of peptides from N–terminal coil 2B of keratins: The isotopic envelopes of (A) peptide "313– M_{310} – L_{317}" (K8) and (B) peptide "277– I_{275} – T_{280}" (K18) after 10 s of exchange at pH 8.4 are compared for HMO and tetramers of HRO. Also shown: the maximum possible exchange (MAX) and/or minimum possible exchange (IN) isotopic envelopes; see also Materials and Methods.

Figure 6. Overview of patterns of exchange for keratin HMOs: Keratin 8 (A) and keratin 18 (B) in HMOs at pH 9.0. The peptide position in the sequence is shown on the horizontal axis represented by a horizontal bar of length equal to that of the peptide. The position of the bar at the vertical axis marks the fraction exchanged after 10 s of exchange. Values close to 100% indicate fully unprotected regions, i.e., regions of high flexibility, whereas values close to 0% represent protected regions, indicating a stable structure. Y–axis error bars are the square root of the sum of variances of the subtracted values obtained from at least three independent experiments. Whenever a split isotopic envelope (see text) was observed, the fraction of exchange was separately calculated for both envelopes and shown by the color code: purple for the more stable structural form and orange for the unfolded form. Black denotes peptides for which no split was observed. Small differences in the exchanged fraction obtained for different charge forms or overlapping peptides underscore the good internal consistency of the data.

Figure 7. Isotopic envelopes for the N–terminal head peptide: peptides from K8 (A) and K18 (B) after 10 s of exchange are shown and compared for HMOs and HRO tetramers and filaments. Also shown: maximum possible exchange (MAX) and/or minimum possible exchange (IN); see Materials and Methods. Isotopic envelopes in these peptides show split in HMOs, indicating the coexistence of at least two different structural forms of the protein in solution.

Figure 8. Schematic representation of structured and unstructured regions of keratin HMOs: localization of structured (blocks) and unstructured (wires) regions in K8 and K18 HMOs in the folded (X) and unfolded (Y) forms. The unfolded forms retain short elements of stable coiled–coils, expanding in the folded form when supported by the head (K8 and K18) and/or tail (K18) regions (color code – heads, tails: black; linkers: dark blue; coil 1A: red; coil 1B: blue; coil 2A: green; coil 2B: yellow).

Figure 9. HMOs versus HROs: differences in the fraction of exchanged amide protons for peptides of keratin 8 (A) and keratin 18 (B) measured between the folded form present in homomeric preparations (HMO) and heteromeric form (HRO) after 10 s of exchange, at pH 8.4. The position of a peptide in the sequence is shown on the horizontal axis represented by a horizontal bar of the length equal to the length of the peptide. The position of the bar at the vertical axis marks the result of the subtraction of the fraction exchanged (in %) in the folded form of HMOs from the fraction exchanged in HROs. Error bars are calculated by the square root of the sum of variances of the subtracted values of the subtracted data points. Some peptides of special interest are marked with a tag indicating the position of their center of the protein sequence.

Supplementary Figure S1. Gel electrophoretic analysis of recombinant keratins K8 and K18. Proteins reconstituted into 2mM Tris–HCl, pH 9.0 were taken for analysis on 10% SDS–polyacrylamide gels (5µg each). Lane 1, K8; Lane 2, K18; Lane 3, mixture of K8: K18 in equimolar ratio. Arrowhead, start of separating gel; Arrow at the end denotes the “running front”.

Supplementary Figure S2. Relative deuterium uptake in keratin HROs at pH 9.0: fraction of exchange (% deuteration) of amide protons in peptides from keratin 8 (A) and keratin 18 (B) in heteromeric complex (HROs), at pH 9.0. Protein domains are marked by gray rectangles for coil regions. The position of a peptide in the sequence is shown on the horizontal axis represented by a horizontal bar of the length equal to the length of the peptide. The position of the bar at the vertical axis marks the fraction exchanged after 10 s of exchange.

Supplementary Figure S3. Isotopic envelopes of peptides from K8 coil 1A: peptides 95.5 and 98 (A, B) at various pH values and time points, as indicated. Panels (iii), (iv) include bimodal fits at 80 s, pH 7.5, and 10 s, pH 8.4, which allows measurement of mass centers and relative populations, corresponding to forms “X” (purple) and “Y” (orange), respectively. Mass centers and relative populations of forms A and B in triplicate experiments, along with SD values, measured for filaments at pH 7.5 (red) and tetramers at pH 8.4 (blue), are shown in Supplementary figure S3a. The structural properties of the coil 1A region in K8 differ in filaments and tetramers (see text).

Supplementary Figure S3a. Panels showing mass centers and relative populations of forms “X” and “Y” in triplicate experiments of peptides 95.5 (A) and 98 (B), along with SD values, measured for filaments at pH 7.5 (red) and tetramers at pH 8.4 (blue).

Supplementary Figure S4. Isotopic envelope profiles of peptides “Y_{282}–L_{289}” and “Q_{290}–L_{300}”: panels (i), (ii) represent the isotopic envelopes at pH 7.5 after 10 s and 80 s of exchange, respectively; (iii), (iv) at pH 8.4 and pH 9 after 10 s of exchange; and panel (v) depicts the maximum exchange.

Supplementary Figure S5. Isotopic envelope profiles of peptide “Q_{153}–L_{159}” from coil 1B of K18: panels (i), (ii) represent the isotopic envelopes at pH 7.5 after 10 s and 80 s of exchange, respectively; (iii), (iv) at pH 8.4 and pH 9 after 10 s of exchange; and panel (v) depicts the maximum exchange.

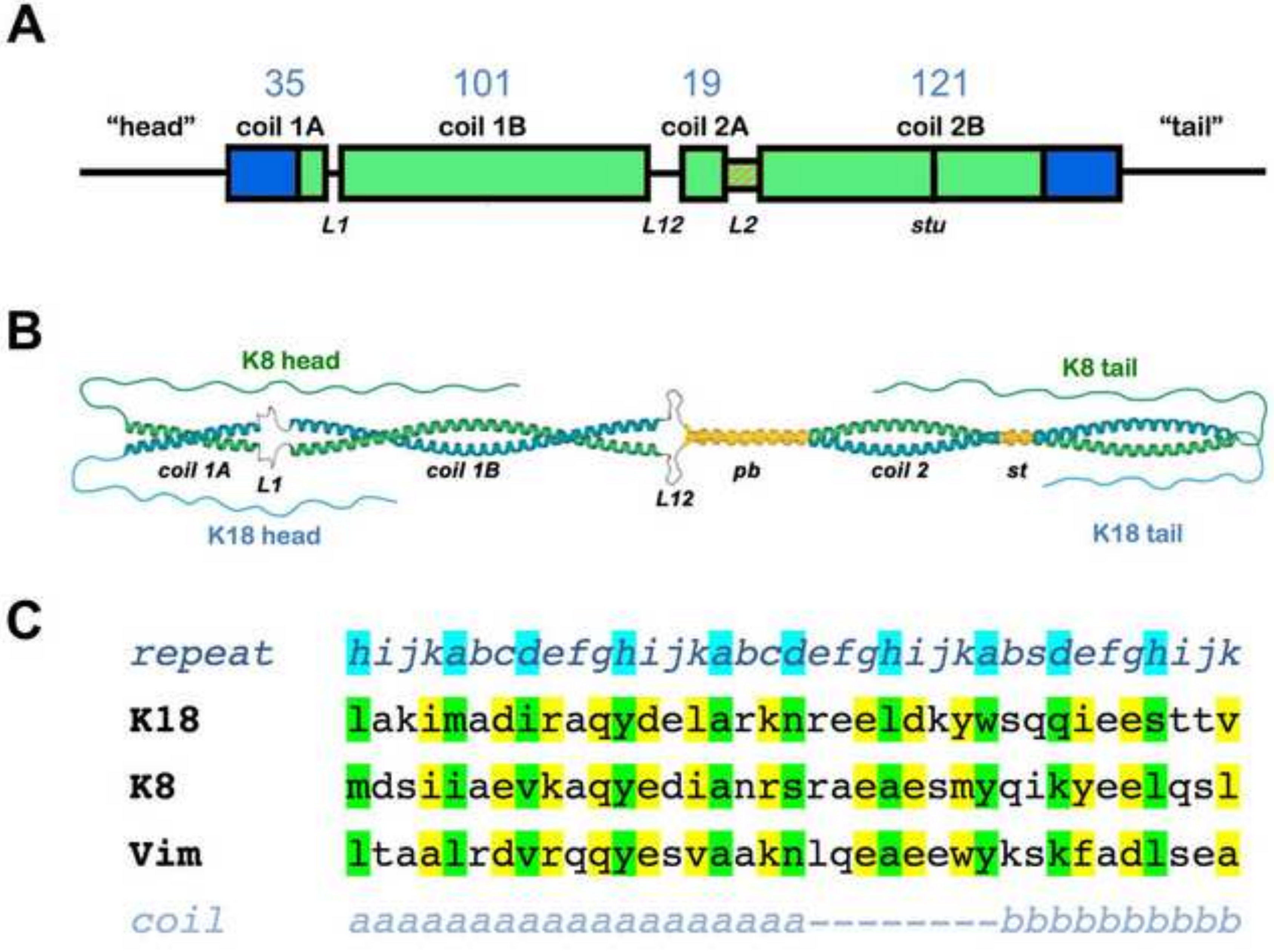
A
35
101
19
121
"head"
coil 1A
coil 1B
coil 2A
coil 2B
"tail"
L1
L12
L2
stu
B
K8 head
K8 tail
coil 1A
L1
coil 1B
L12
pb
coil 2
st
K18 head
K18 tail
C
repeat hijkabcdefghijkabcdefghijkabsdefghijk
K18 lakimadiraqydelarknreeldkywsqqieesttv
K8 mdsiiaevkaqyedianrsraeaesmyqikyeelqsl
Vim ltaalrdvrqqyesvaaknlqeaeewykskfadlsea
coil aaaaaaaaaaaaaaaaaaa--------bbbbbbbbbb

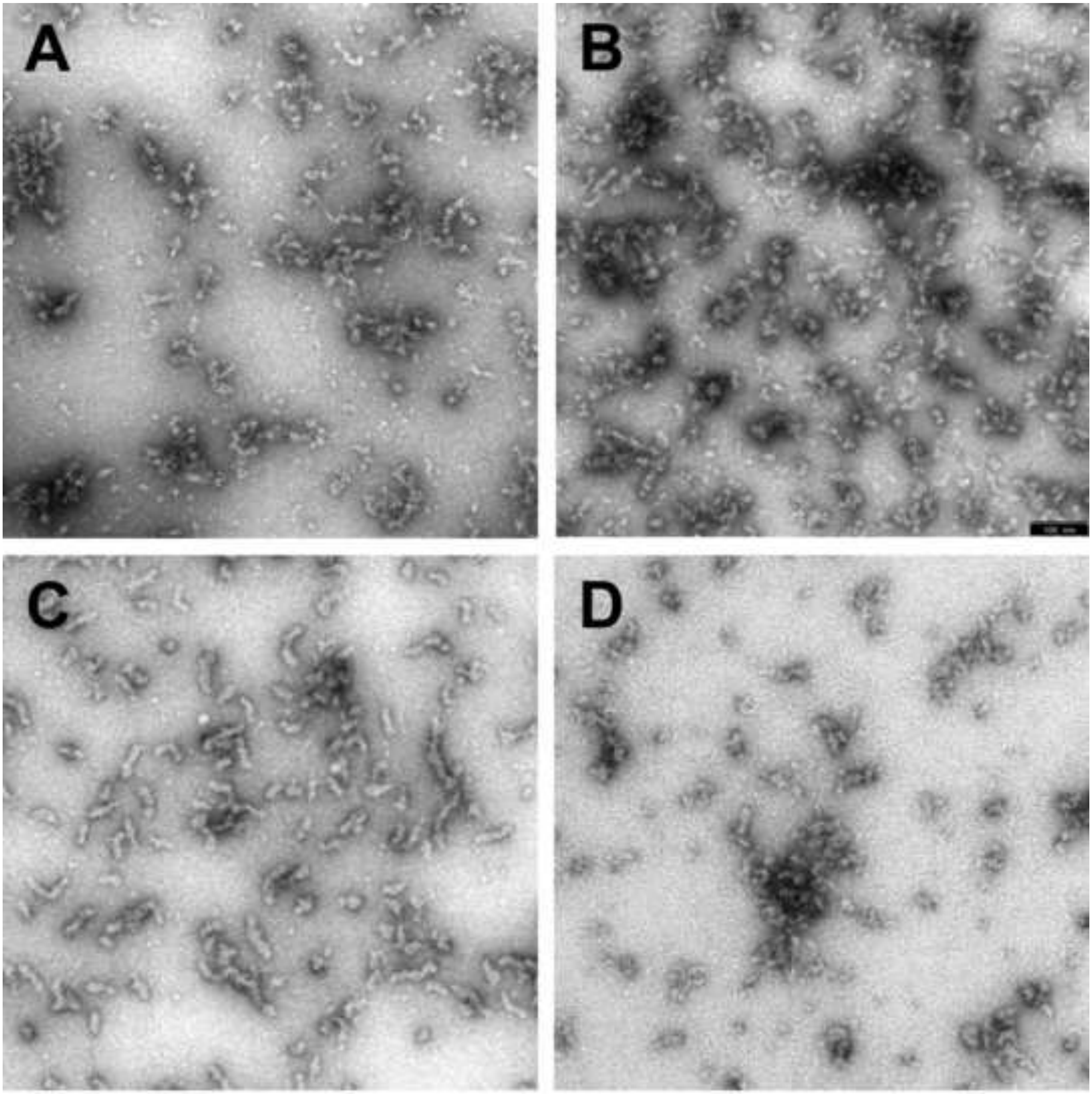
A
B
C
D

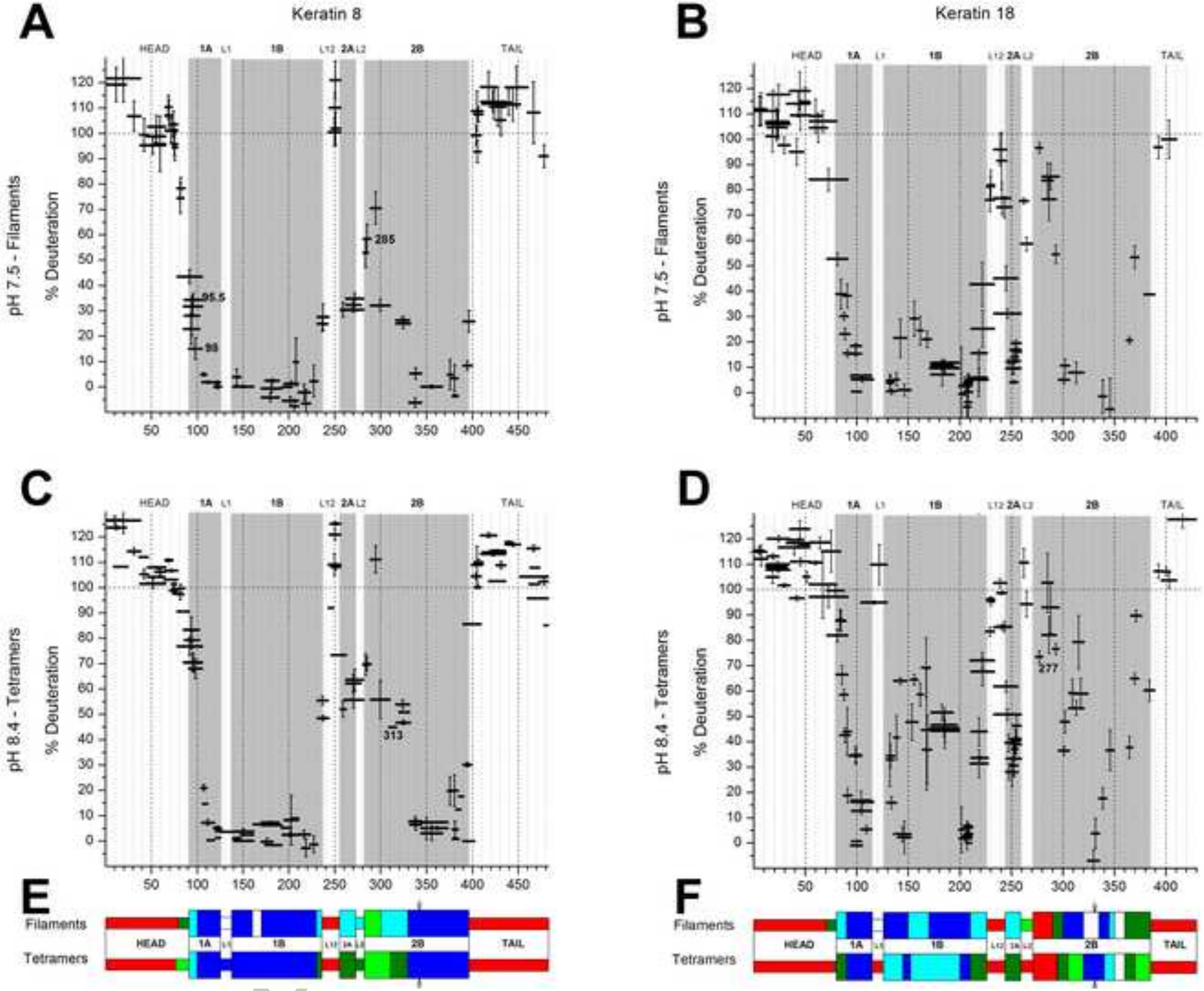
A
Keratin 8
B
Keratin 18
HEAD
1A
L1
1B
L12
2A
L2
2B
TAIL
pH 7.5 - Filaments
% Deuteration
0
10
20
30
40
50
60
70
80
90
100
110
120
50
100
150
200
250
300
350
400
450
95.5
98
285
C
D
pH 8.4 - Tetramers
313
277
E
F
Filaments
Tetramers

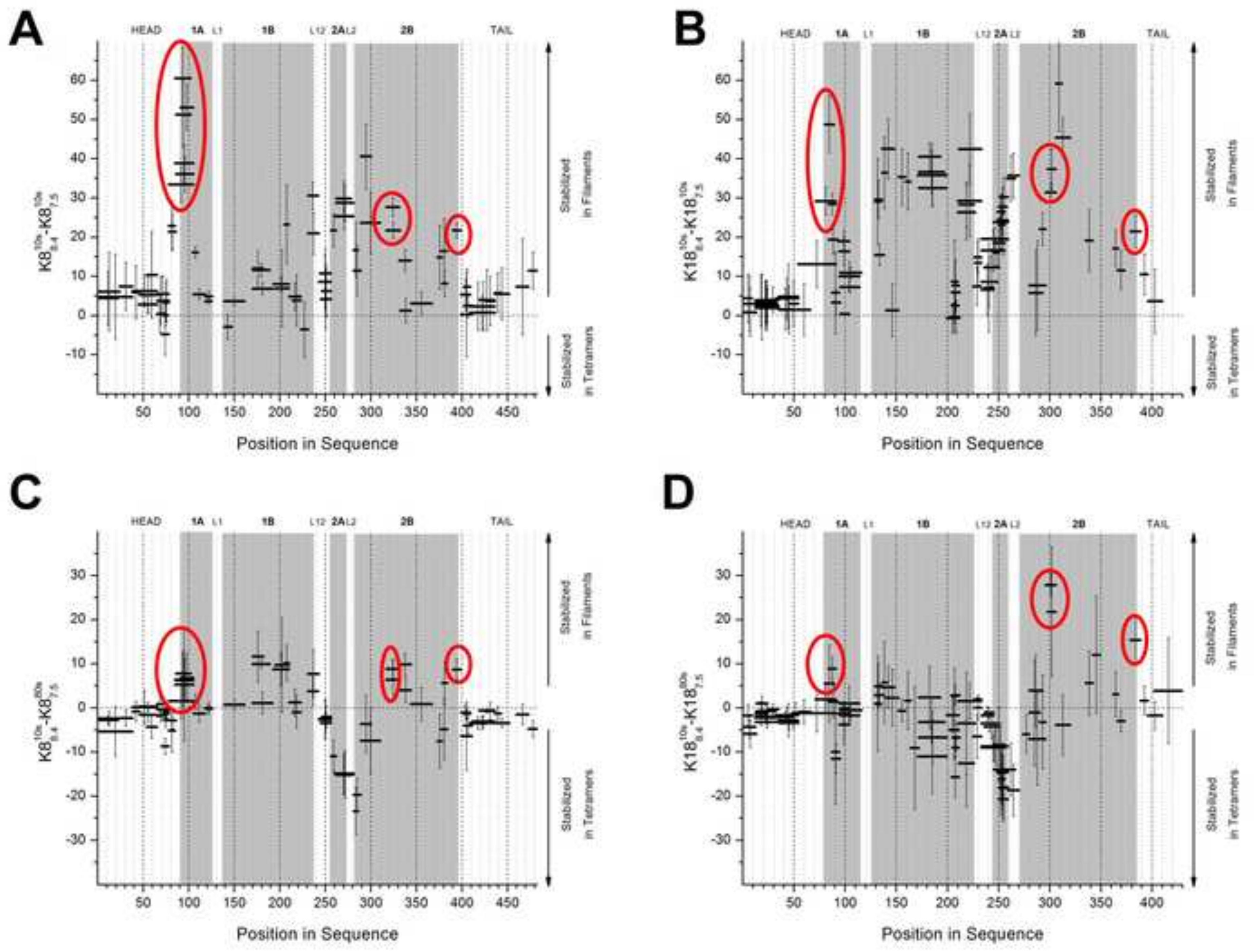
A
B
C
D
HEAD
1A
L1
1B
L12
2A
L2
2B
TAIL
$K8^{10s}_{8.4}$-$K8^{10s}_{7.5}$
$K18^{10s}_{8.4}$-$K18^{10s}_{7.5}$
$K8^{10s}_{8.4}$-$K8^{60s}_{7.5}$
$K18^{10s}_{8.4}$-$K18^{60s}_{7.5}$
Position in Sequence
Stabilized in Filaments
Stabilized in Tetramers
-10
0
10
20
30
40
50
60
-30
-20
50
100
150
200
250
300
350
400
450

ACC

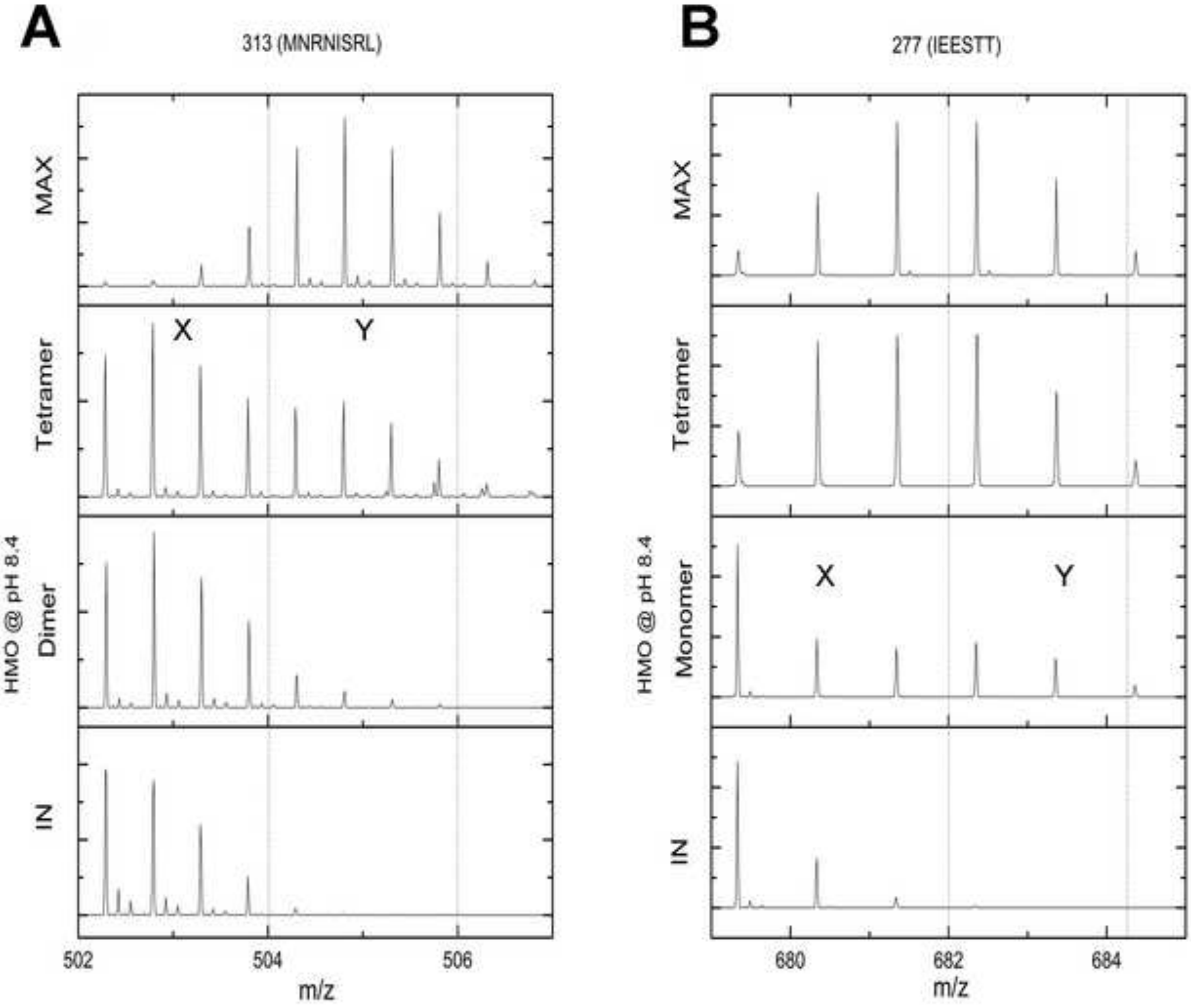
A
313 (MNRNISRL)
MAX
Tetramer
X
Y
HMO @ pH 8.4
Dimer
IN
502
504
506
m/z
B
277 (IEESTT)
MAX
Tetramer
HMO @ pH 8.4
Monomer
X
Y
IN
680
682
684
m/z

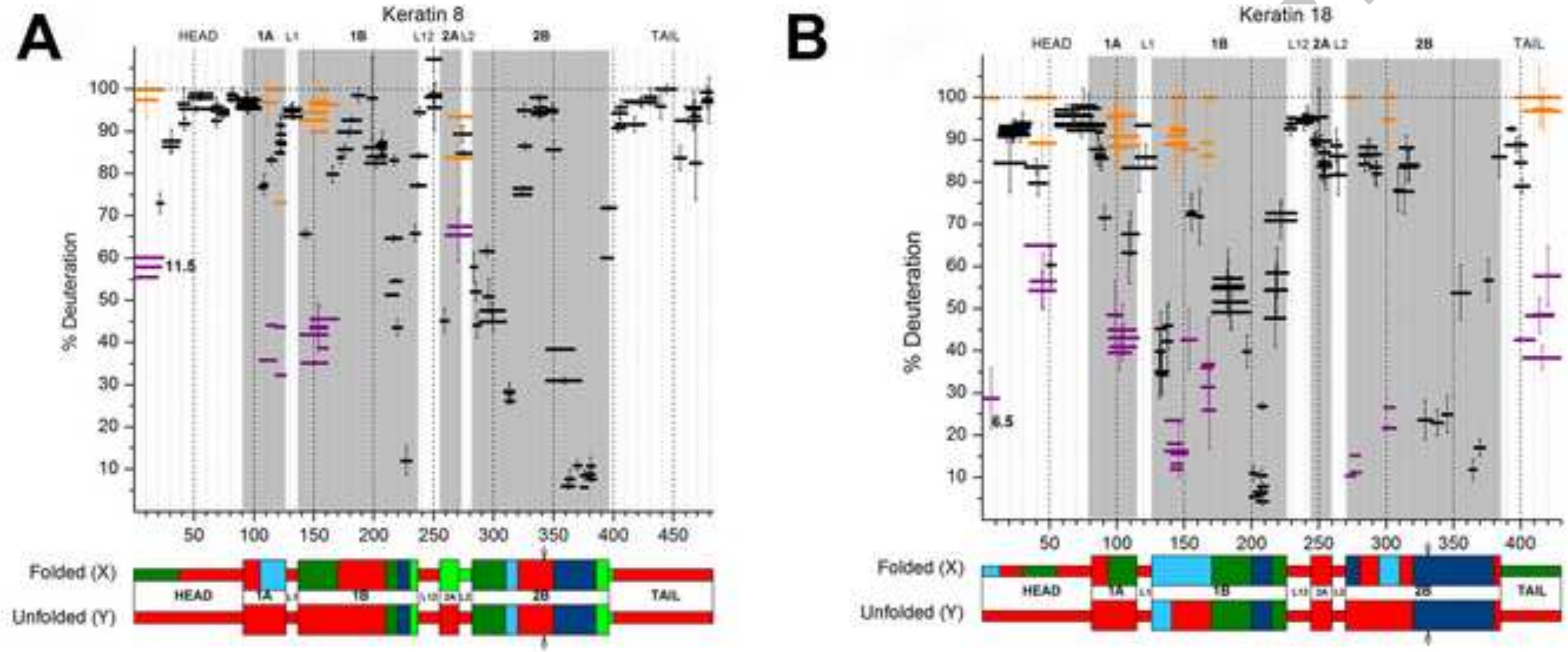
A
Keratin 8
HEAD
1A
L1
1B
L12
2A
L2
2B
TAIL
% Deuteration
11.5
Folded (X)
Unfolded (Y)
B
Keratin 18
6.5

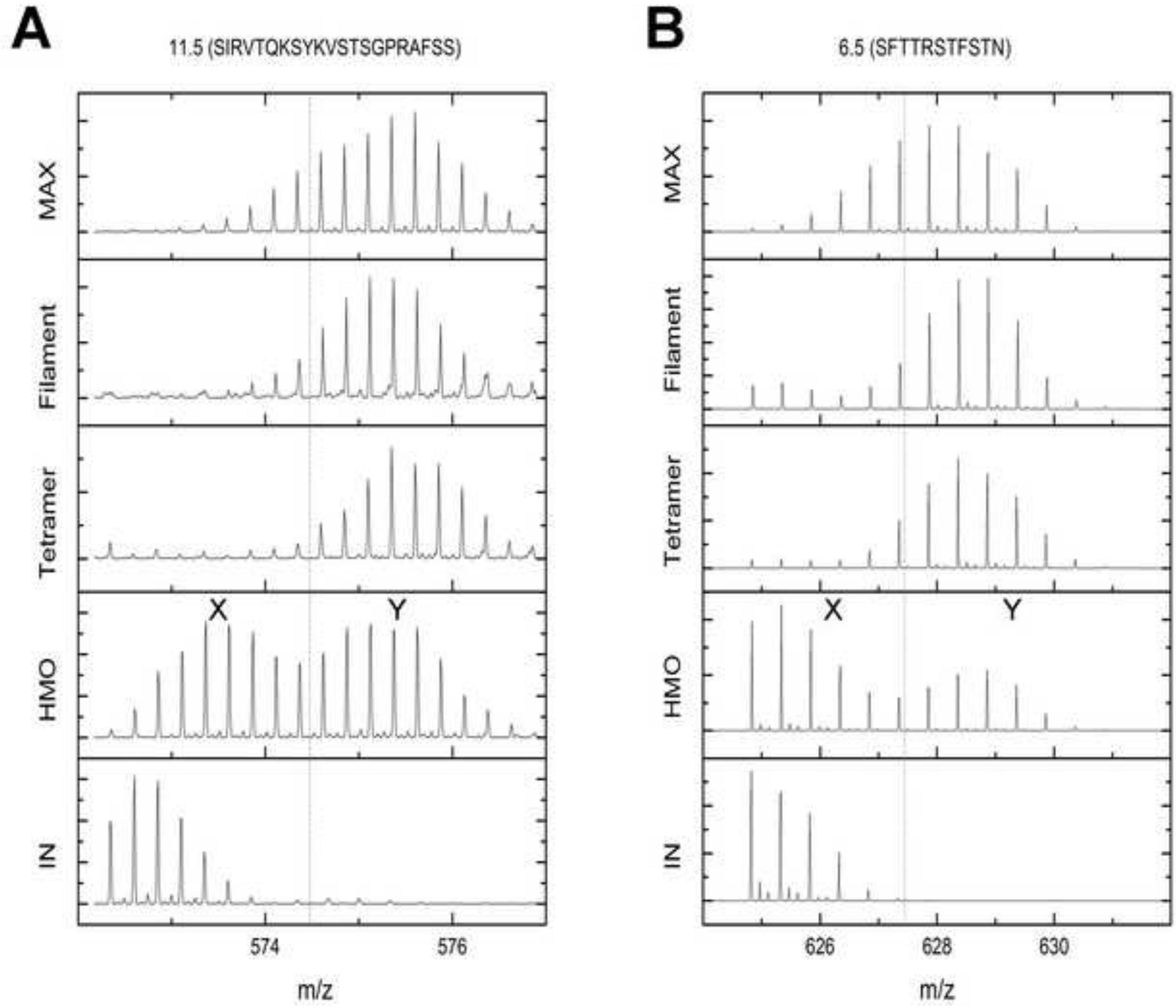
A
11.5 (SIRVTQKSYKVSTSGPRAFSS)
MAX
Filament
Tetramer
X
Y
HMO
IN
574
576
m/z
B
6.5 (SFTTRSTFSTN)
MAX
Filament
Tetramer
X
Y
HMO
IN
626
628
630
m/z

Ac

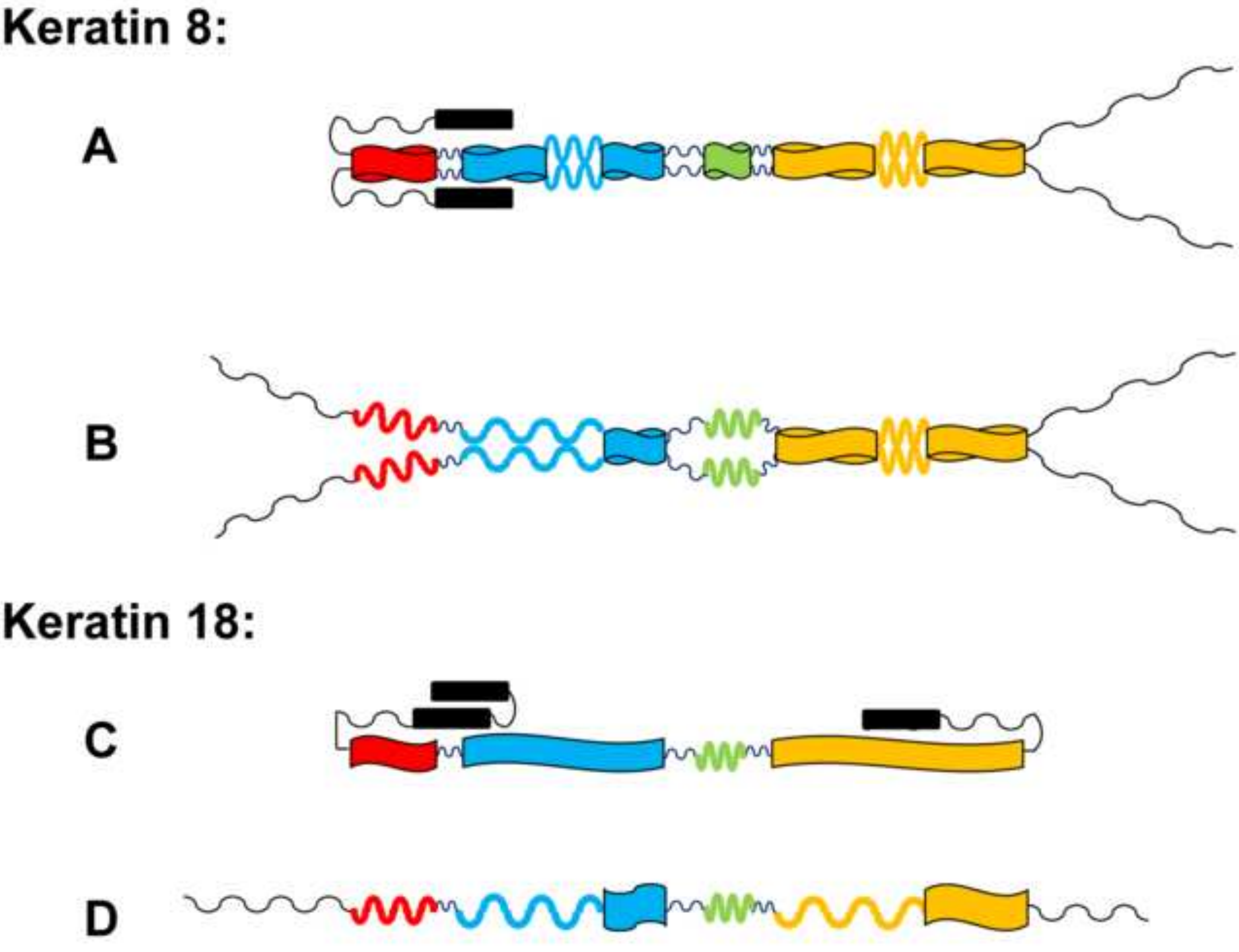
Keratin 8:
A
B
Keratin 18:
C
D

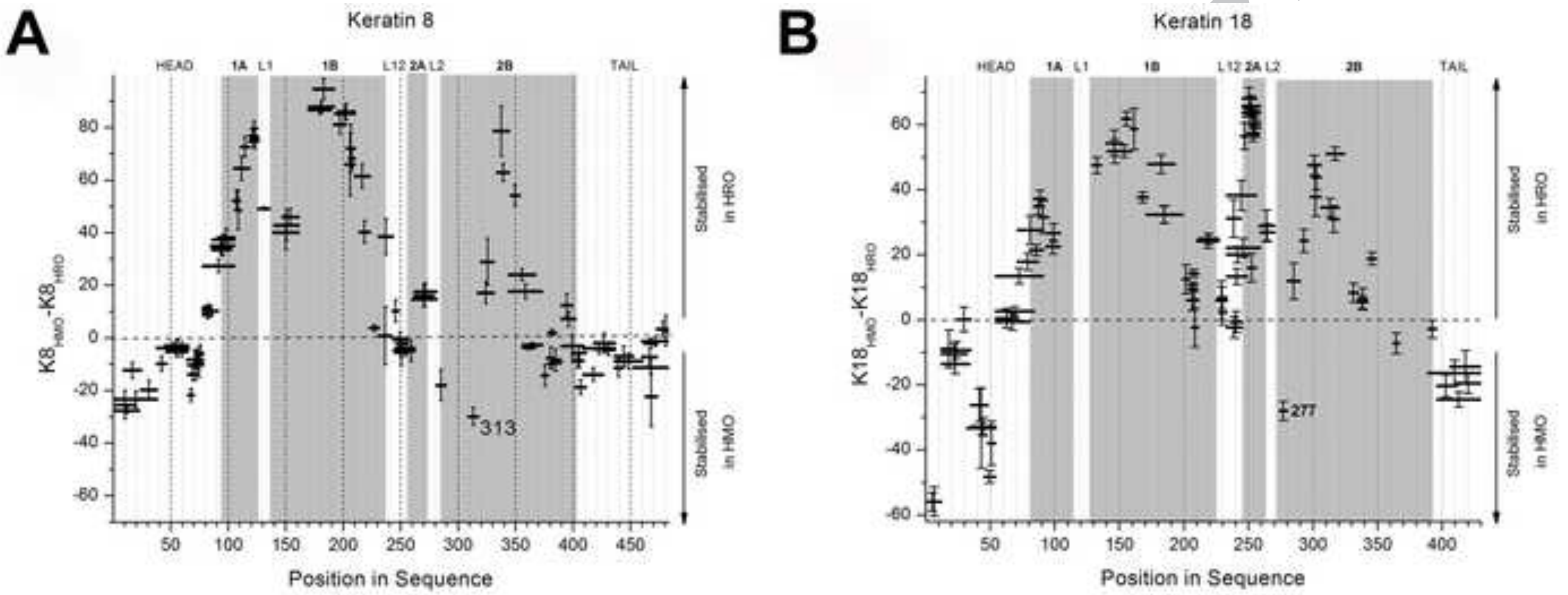
A
Keratin 8
HEAD
1A
L1
1B
L12
2A
L2
2B
TAIL
80
60
40
20
0
-20
-40
-60
K8$_{HMO}$-K8$_{HRO}$
313
Stabilised in HRO
Stabilised in HMO
50
100
150
200
250
300
350
400
450
Position in Sequence
B
Keratin 18
HEAD
1A
L1
1B
L12
2A
L2
2B
TAIL
60
40
20
0
-20
-40
-60
K18$_{HMO}$-K18$_{HRO}$
277
Stabilised in HRO
Stabilised in HMO
50
100
150
200
250
300
350
400
Position in Sequence

Table 1

Association state of keratins K8, K18, and K8/K18 by sedimentation velocity ultracentrifugation as depending on a prior concentration-dilution step

Protein	pH[a]	$s1_{20,w}$ (S)[d]	$s2_{20,w}$ (S)[d]	s1 species [%] (concentration-dilution step)	
				without[b]	with[c]
K8	9.0.	3.7	17	88	--
K8	9.0	3.9 \ 3.7	12 \ 28	97	39
K18	9.0.	2.8	9-14	87	--
K18	9.0.	2.6 \ 2.7	9 \ 25	92	31
K8/18	9.0.	4.4	5.9	72	--
K8/18	9.0.	4.6 \ 4.3	6.5 \ 5.9	76	72
K8/18	8.4	4.7	6.6	69	--
K8/18	8.4	4.8 \ 4.6	6.7 \ 6.5	76	73

[a] 2 mM Tris-HCl, pH 9.0; 5 mM Tris-HCl, pH 8.4.

[b] Amount of protein in s1 in percent of total protein recorded in the run without a concentration step.

[c] Amount of protein in s1 in percent of total protein recorded in the run after the protein had been first concentrated to 3 g/l and then diluted back to 0.2 g/l for centrifugation analysis.

[d] In the experiments with concentration step, the number before the backslash refers to the *s*-value of the protein before concentration, the number after the backslash refers to the *s*-value obtained after the sample was concentrated to ~ 3 g/l and then diluted back with the corresponding buffer to 0.2 g/l.